Malignant Lesions of the Central and Posterior Skull Base

Ilona M. Schmalfuss

Contents

I. M. Schmalfuss (✉)
Department of Radiology,
Malcolm Randall VA Medical Center
and University of Florida College of Medicine,
1601 SW Archer Road, Gainesville, FL 32608, USA
e-mail: Ilonaschmalfuss@yahoo.com

Abstract

Imaging interpretation of skull base lesions can be challenging because of their infrequent occurrence, the complex nature of the skull base and the ability of normal anatomical variations to mimic pathology. Since the majority of skull base lesions are accidentally detected and inaccessible for biopsy, the clinicians heavily rely upon the accurate image interpretation by the radiologist. The main goals of the image analysis are to distinguish normal anatomical variations form true pathology, recognize medically treatable conditions and to differentiate benign "do-not-touch" lesions from malignant processes that might require aggressive treatment. The imaging features and preferential location of the different malignant skull base lesions and their benign counterparts will be discussed in this chapter. After the diagnosis of a malignancy is established, the radiologist's main role is the delineation of the extent of the suspected malignant skull base lesion for treatment planning.

1 Introduction

Evaluation of skull base lesions is challenging. On the one hand, the skull base is not directly accessible for clinical evaluation, and an underlying lesion is suspected based on neurological deficits. On the other hand, cross-sectional radiological studies are excellent in demonstrating a skull base lesion and its extent, but their evaluation is intimidating to the majority of radiologists. There are three main reasons for the intimidation of radiologists: The anatomical

R. Hermans (ed.), *Head and Neck Cancer Imaging*, Medical Radiology. Diagnostic Imaging,
DOI: 10.1007/174_2011_386, © Springer-Verlag Berlin Heidelberg 2012

complexity of the skull base, the ability of normal anatomical structures to mimic pathology and the rarity of skull base lesions preventing dedicated training throughout residency and even during fellowship. In addition, inappropriate choice of an imaging study, imaging parameters and/or sequences may amplify the insecurity of the radiologist.

Recognition of anatomical mimics and of medically treatable conditions is essential as the majority of skull base lesions are inaccessible for biopsy. The biopsy route may extend through normal pertinent anatomical structures, such as inner ear in case of a petrous apex lesion, or may need to be performed through the intracranium. Differentiation of malignant from benign lesions is also critical as a different surgical intervention may apply, the lesion might be vascular in nature preventing a biopsy, or occasionally treatment might be conducted without a tissue diagnosis, e.g. radiation therapy in case of paragangliomas. In addition, determination of the exact origin and extent of a lesion is crucial for radiation therapy and even more for surgical planning purposes. All these points will be addressed in this chapter.

2 Anatomy

The anatomy of the skull base is very complex; not only do the bony structures play an important role but also the cranial nerves and vasculature coursing through it. Knowledge of the location of the different neural and vascular foramina and channels, as well as of the different neuronal connections, can therefore explain the wide range of clinical symptoms and facilitate the detection of extracranial tumor spread.

The skull base is formed by the ethmoid, sphenoid, occipital, frontal and temporal bones. It is divided into three regions: anterior, central and posterior skull base. Only the central and the posterior skull base will be discussed in this chapter as the anterior skull base is included in "Neoplasms of the Sinonasal Cavities". The distinction of the central to posterior skull base is ambiguous as the roof of the petrous apex represents part of the central skull base, while the posterior margin borders the posterior skull base. Since the majority of the malignant petrous apex lesions are surgically approached from the posterior fossa, the petrous apex will be included in the posterior skull base in the subsequent discussion.

2.1 Central Skull Base

The sphenoid bone forms the middle portion of the central skull base. It is subdivided into the central sphenoid body housing the sella and the sphenoid sinuses, the greater sphenoid wings forming the boundary to the anterior skull base, the lesser sphenoid wings and the pterygoid processes that are protruding below the skull base and serve as attachments for the medial and lateral pterygoid muscles. Parts of the temporal bones compose the lateral portions of the central skull base and are formed by the mastoid, tympanic, petrous and squamous bones. The greater sphenoid wing is connected via the sphenosquamous suture and the petrosphenoidal fissure with the squamous and petrous portions of the temporal bone, respectively. The anterior portion of the squamous bone creates the lateral border of the central skull base while the petrous bone together with the clivus form the anterior boundary of the posterior skull base. The petrous bone and the clivus are separated by the petro-occipital fissure.

The central skull base represents the floor of the middle cranial fossa which is primarily filled with the temporal lobes laterally and the cavernous sinuses medially. The cavernous sinuses are located between the dura and the periostium of the body of the sphenoid bone and between the superior orbital fissure anteriorly and the petrous apex posteriorly. Each cavernous sinus contains a complex venous plexus surrounding the internal carotid artery and the cranial nerve VI. The cranial nerve VI enters the cavernous sinus through a small bony channel within the medial petrous apex called Dorello's canal. The cranial nerves III–V are actually located within the dural leaflet that form the lateral boundary of the cavernous sinus rather than within the cavernous sinus itself. These cranial nerves and the internal carotid artery exit the intracranium through different foramina located within the central skull base.

The superior orbital fissure and the optic canal are the most anterior openings of the central skull base. The optic nerve, optic nerve sheath and the ophthalmic artery course through the optic canal. The cranial nerves III, IV and VI as well as the lacrimal, frontal and nasociliary branches of the first division of the trigeminal nerve (V1) exit the cavernous sinus into the orbital apex through the superior orbital fissure. The foramen rotundum is located just inferior to the

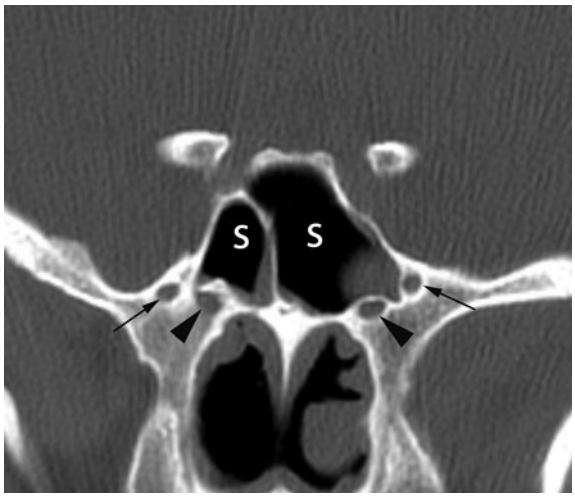

Fig. 1 Coronal CT image displayed in bone window demonstrating the relationship between the foramen rotundum (*arrows*) and vidian canal (*arrowheads*) to each other and the sphenoid sinus (*s*) within the central skull base

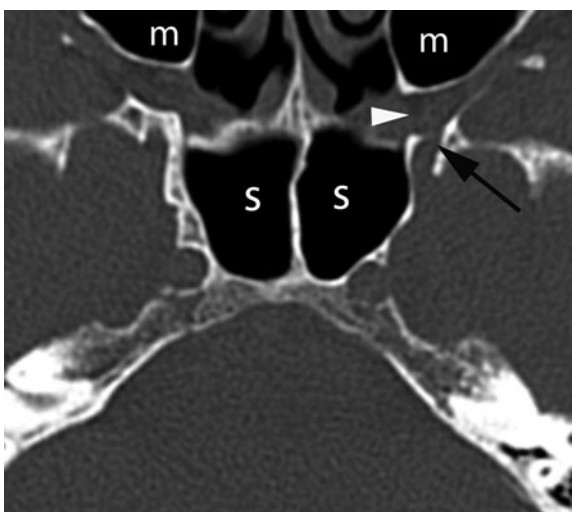

Fig. 2 Axial CT image displayed in bone window illustrates the communication of the foramen rotundum (*arrow*) with the pterygopalatine fossa (*arrowhead*) located immediately posterior to the maxillary sinus (*m*). *s*, Sphenoid sinus

Fig. 3 Axial CT image of the central skull base displayed in bone window shows the larger foramen ovale (*black arrows*) on each side and the smaller foramen spinosum (*black arrowheads*) posterior lateral to it. Both assume an oval shape. The *white arrowheads* demarcate the vidian canal that extends from the pterygopalatine fossa (*white arrows*) to the foramen lacerum within the petrous apex (not demonstrated at this level). *s* Sphenoid sinus

superior orbital fissure and houses the second division of the trigeminal nerve (V2) (Fig. 1). The foramen rotundum communicates anteriorly with the pterygopalatine fossa where a few ganglionic branches leave V2 to travel to the pterygopalatine ganglion (Fig. 2; Moore et al. 1999). V2 gives off the zygomatic and the posterior superior alveolar nerves and then continues anteriorly as the infraorbital nerve within the infraorbital canal. The third division of the trigeminal nerve (V3) courses through the central skull base within the foramen ovale situated posterior and lateral to the foramen rotundum (Fig. 3). V3 travels inferiorly to enter the masticator space. Just superomedial to the foramen ovale is a groove within the central skull base, located immediately posterior to the cavernous sinus, containing the Meckel's cave. The Meckel's cave houses the trigeminal ganglion anteroinferiorly, where the three divisions of the trigeminal nerve are merging together, and the trigeminal cistern (Kaufman and Bellon 1973; Williams et al. 2003). The trigeminal ganglion gives rise to multiple individual rootlets that course superiorly through the trigeminal cistern. The individual rootlets give the trigeminal cistern a speckled appearance on coronal high resolution images before they merge together to form the main trunk of the trigeminal nerve just posterior to the trigeminal cistern.

The foramen spinosum and the lacerum portion of the carotid canal are the most posterior foramina of the central skull base. The foramen spinosum is located just posterolateral to the foramen ovale and contains the middle meningeal artery, a distal branch of the external carotid artery, and the meningeal branch of the facial nerve (Fig. 3). The middle meningeal artery branches off into multiple small vessels

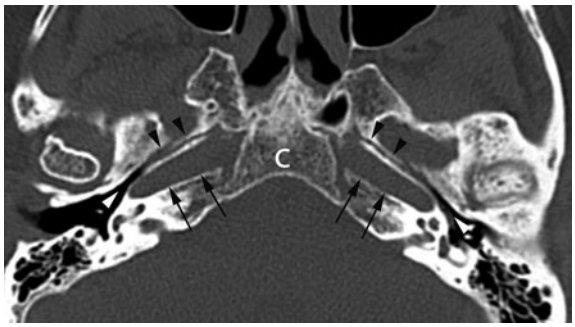

Fig. 4 Axial CT image displayed in bone window illustrates the close relationship between the clivus (*c*) centrally and the internal carotid artery canal within the petrous apex laterally (*arrows*). The Eustachian tube courses parallel to the internal carotid artery canal through the petrous bone (*black arrowheads*). The *white arrowheads* demarcate the Eustachian tube openings within the middle ear cavities

intracranially that form grooves within the superior surface of the central skull base and along the inner table of the frontal and anterior parietal skull. The lacerum portion of the carotid canal is located more medially within the body of the sphenoid bone, at the junction of the petrous apex and clivus (Tauber et al. 1999). It represents the exit site of the internal carotid artery from the carotid canal within the petrous portion of the temporal bone (Fig. 4). The internal carotid artery continues superiorly as the carotid siphon to lie within a sigmoid-shaped groove along the sphenoid bone within the cavernous sinus. The internal carotid artery exits the cavernous sinus medial to the anterior clinoid process. The vidian canal courses inferior to the carotid siphon within the sphenoid bone forming a direct communication between lacerum portion of the carotid canal and the pterygopalatine fossa (Fig. 3; Chong and Fan 1998). It contains the vidian nerve that is composed of preganglionic parasympathetic fibers of the greater superficial petrosal nerve, the postganglionic sympathetic fibers of the deep petrosal nerve and sensory fibers from the cranial nerve VII.

2.2 Posterior Skull Base

The posterior skull base is shaped like a cup. The clivus and the petrous apex create the anterior boundary while the occipital bone forms the posterior and inferior borders of the posterior skull base. The lateral boundary of the posterior skull base is established by the occipital bone posteriorly and the mastoid and petrous portions of the temporal bone superoanteriorly and inferoanteriorly, respectively. The occipitomastoid suture connects the occipital bone with the mastoid portion of the temporal bone. The different anatomical structures of the posterior fossa create numerous grooves, crests and foramina within the posterior skull base.

The cerebellar hemispheres cause two indentations along the posterior surface of the posterior skull base with a midline internal occipital crest in between. The occipital crest provides the attachment for the falx cerebelli and extends from the foramen magnum to the internal occipital protuberance. One vertical and two horizontal grooves extend superiorly and laterally from the internal occipital protuberance housing the superior sagittal sinus and the transverse sinuses, respectively. The horizontal grooves are extending anteroinferiorly to continue as the sigmoid sulci that contain the sigmoid sinus on each side. The sigmoid sinus subsequently enters the jugular foramen and continues through the skull base into the neck as the internal jugular vein.

The jugular foramen and the foramen magnum are the largest openings of the posterior skull base. The jugular foramen lies at the posterior end of the petrooccipital fissure and is bordered by the petrous bone of the temporal bone anteriorly and the occipital bone posteriorly. It is partially subdivided by the jugular spine into two compartments: the pars venosa and the pars nervosa (Fig. 5; Inserra et al. 2004; Sen et al. 2001). Only occasionally the bony jugular spine continues as a fibrous or osseous septum posteriorly to completely separate these two compartments. The pars venosa lies posterolateral and contains the internal jugular bulb laterally and the cranial nerves X and XI medially (Fig. 5). The pars nervosa is located anteromedially and contains the cranial nerve IX medially and often the inferior petrosal sinus laterally (Fig. 5). The internal carotid artery enters the skull base anterior to the jugular foramen (Fig. 5). Therefore, all three of these cranial nerves lie between the internal jugular vein and the internal carotid artery below the skull base, with the cranial nerve IX being the most anterolateral and the cranial nerve XI the most posteromedial in position.

The cranial nerve XI is very unique as it extends through the posterior skull base twice. Once to exit

Fig. 5 Axial CT image of the right jugular fossa displayed in bone window shows the jugular spine (*arrow*) dividing the jugular foramen into the pars venosa (*pv*) laterally and pars nervosa (*pn*) medially. The internal carotid artery (*c*) lies anterior to the pars venosa (*pv*)

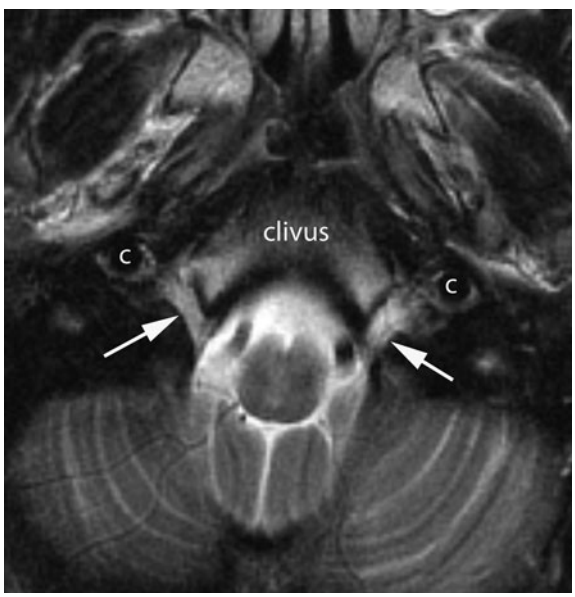

Fig. 6 Axial T2-weighted image through the lower clivus demonstrates the oblique course of the hypoglossal canal (*arrows*) along the lateral edge of the clivus on each side. The exit of the hypoglossal canal (*arrows*) is in close proximity to the internal carotid artery (*c*)

the skull base through the jugular foramen as mentioned above and once to enter the posterior cranial fossa through the foramen magnum as parts of its fibers originate from the cervical spinal cord. The remaining cranial nerve XI fibers originate from the medulla oblongata and merge with the cervical spinal cord fibers at the foramen of magnum. The cranial nerves XI lie posterior to the vertebral arteries that ascend from cervical to intracranial through the foramen mangum. The vertebral arteries give rise to the posterior cerebellar arteries that course posteroinferiorly to supply the inferior cerebellar hemispheres. In turn, the paired posterior spinal arteries arise either from the intracranial portion of the vertebral arteries or occasionally from the posterior cerebellar arteries and continue inferiorly through the foramen magnum to supply the spinal cord.

The posterior skull base has few additional, smaller openings. The porus acusticus is the medial opening of the internal auditory canal along the posterior surface of the petrous bone. It contains the cranial nerves VII and VIII as well as branches of the anterior inferior cerebellar artery that supply the inner ear. Inferior and posterior to it are the openings of the cochlear and vestibular aqueducts, respectively. The vestibular aqueduct courses almost parallel to the posterior margin of the petrous bone between the vestibule and the intracranium and contains the endolymphatic duct. In contrast, the cochlear aqueduct runs almost parallel to the internal auditory canal between the basal turn of the cochlea and the intracranium within the inferior aspect of the petrous bone and transmits the perilymphatic duct (Mukherji et al. 1998). Even more inferiorly within the petrous bone is the hypoglossal foramen located just inferomedial to the jugular foramen (Fig. 6). It contains the cranial nerve XII, the hypoglossal venous plexus and a meningeal branch of the ascending pharyngeal artery. Below the skull base, the cranial nerve XII continues inferiorly between the internal carotid artery and the internal jugular vein.

3 Clinical Presentation

Only few skull base lesions present with specific, disease-related symptoms that significantly help to narrow the differential diagnosis. The Gradenigo's triad represents one of them and is characterized by

Table 1 Clinical symptoms of cranial nerve palsies

Cranial nerve	Symptoms
Cranial nerve III (oculomotor nerve)	Diplopia due to inability to move the ipsilateral eye superiorly, inferiorly and medially Ptosis Fixed and dilated pupil
Cranial nerve IV (trochlear nerve)	Dilopia due to inability to move the ipsilateral eye inferiormedial
Cranial nerve V (trigeminal nerve)	Loss of sensation or dysaesthesia in the ipsilateral face Ipsilateral loss of jaw clenching and side to side movement
Cranial nerve VI (abducens nerve)	Diplopia due to inability to move the ipsilateral eye laterally
Cranial nerve VII (facial nerve)	Loss of taste in the anterior 2/3 of the tongue Ipsilateral facial drop
Cranial nerve VIII (vestibulocochlear nerve)	Ipsilateral sensorineural hearing loss Dizziness
Cranial nerve IX (glossopharyngeal nerve)	Loss of oropharyngeal sensation Loss of taste and sensation to the posterior 1/3 of tongue
Cranial nerve X (vagus nerve)	Nasal speech due to ipsilateral palatal weakness Hoarseness due to ipsilateral vocal cord paralysis
Cranial nerve XI (spinal accessory nerve)	Weakness and wasting of the ipsilateral sternocleidomastoid and trapezius muscles
Cranial nerve XII (hypoglossal nerve)	Wasting and fasciculation of the tongue Tongue tip deviation to paralyzed side on protrusion

ipsilateral cranial nerve VI paralysis, severe facial pain in V1 distribution and inflammatory disease of the middle ear and/or mastoid air cells (Gradenigo 1904). As the triad indicates, this symptom complex has been associated with extensive acute inflammatory disease of the ear. However, less than 50% of the patients present with all three of these symptoms. In particular, cranial nerve VI palsy has been described as the least reliable clinical sign of the triad making distinction to other skull base entities more difficult (Price and Fayad 2002). Hence, the majority of patients with skull base pathology present with non-specific neurological symptoms related to the mass effect caused by the lesion. These symptoms can be related to cranial nerve dysfunction, vascular compromise or direct compression of the brain or orbital structures. The clinical symptoms of cranial nerve palsies are summarized in Table 1.

4 Normal Anatomical Variations

Normal anatomical variations are asymptomatic and typically discovered incidentally in patients that seek medical attention for an unrelated reason (Schmalfuss and Camp 2008). Asymmetric aeration of the petrous apex is the most common entity that is mistaken for a petrous apex mass, in particular on MR imaging (Fig. 7). CT certainly is easier to interpret in this regard, however, close attention to the imaging characteristics can facilitate the correct diagnosis on MR images as well. In particular, lack of mass effect and increased T1 signal intensity of the fatty bone marrow within the unaerated petrous apex is characteristic (Fig. 7a). Asymmetric accumulation of fluid within the petrous apex air cells will show intermediate T1 and high T2 signal intensity and may be mistaken for a chondrosaroma; however, the lack of mass effect and of contrast enhancement as well as often accompanied fluid within the middle ear cavity and/or mastoid air cells should question such a diagnosis (Schmalfuss 2009).

A high riding jugular bulb or a jugular bulb diverticulum might be mistaken for a mass within the jugular foramen. Close evaluation of all images in the different planes and on the various sequences typically reveals inconsistency of the flow pattern, with the classic flow void seen in at least one plane or on one sequence in such cases.

Mottled fatty replacement of the bone marrow may mimic a diffuse infiltrative process of the skull base that might be impossible to distinguish from lymphoma, leukemia, multiple myeloma or diffuse metastatic disease. Correlation to clinical symptoms, age, gender and history of an underlying malignancy

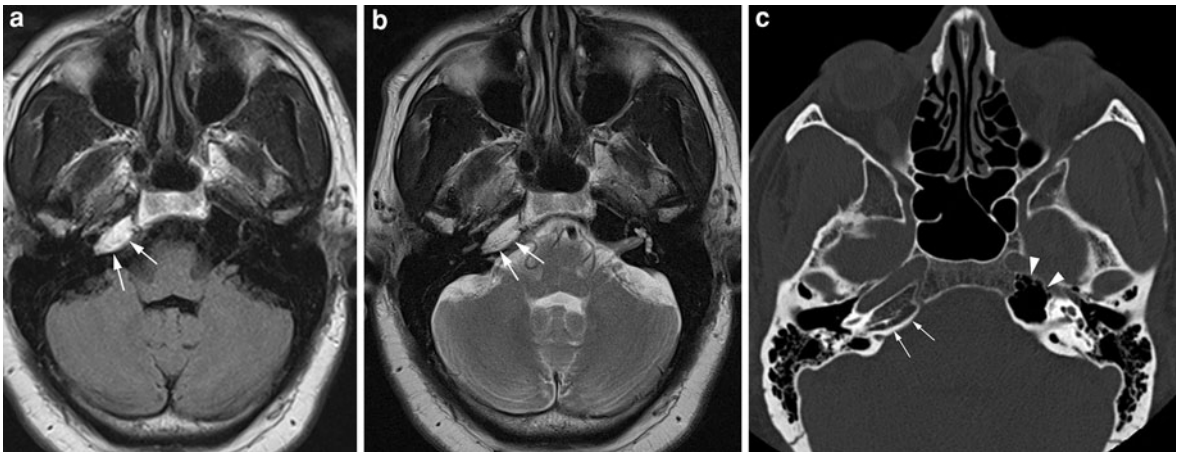

Fig. 7 Axial non-contrast enhanced T1- (**a**) and T2-weighted (**b**) images demonstrate increased signal intensity within the right petrous apex (*arrows* in **a** and **b**) that is often mistaken for a small cholesterol granuloma. The axial CT image displayed in bone window however, reveals the true nature of this "lesion" as it shows preserved diploic trabeculations within the non-aerated petrous apex (*arrows* in **c**) when compared to the aerated petrous apex on the left (*arrowheads* in **c**). The non-aerated petrous apex is increased in T1 signal intensity (*arrows* in **a** and **b**) in this patient due to fatty bone marrow but may also assume lower intensity when red bone marrow is present in this location, e.g. in young patients

might help to develop a risk profile that does or does not warrant further evaluation with bone scan, bone marrow biopsy or cross-sectional follow up.

5 Pathology

The skull base is composed of different tissue components and houses a variety of structures that can serve as the origin of skull base masses. Therefore, the spectrum of possible skull base abnormalities is very broad. Skull base lesions overall are rare, with metastatic disease and lymphoma, accounting for most of the lesions. Primary malignancies of the skull base are even more scarce but can be mistaken for benign lesions, and vice versa, creating a diagnostic dilemma. In addition, some of the benign entities show an aggressive growth pattern that might require more aggressive treatment. Therefore, the discussion of pathology of the skull base will also include benign entities that can be mistaken for, or that need to be treated more like a malignant lesion.

Skull base lesions can be divided into two broad categories: diffuse or localized abnormalities. Diffuse involvement of the skull base may manifest as diffuse replacement of the bone marrow or as multi-focal lesions. Localized lesions in turn can be subdivided into region specific and region-non-specific entities. This approach in evaluation of skull base abnormalities is an important starting point. The exact location of the lesion together with its imaging characteristics, patient's demographics and clinical presentation might then further narrow the differential diagnostic considerations.

5.1 Malignant Lesions Causing Diffuse or Multi-focal Skull Base Involvement

Multiple myeloma, lymphoma, leukemia and metastatic disease are the main malignant entities able to cause diffuse replacement of the bone marrow or multifocal involvement of the skull base (Figs. 8, 9). Often, the skull and the visualized portions of the cervical spine are also affected (Fig. 8a). Although any primary cancer can metastatize to the skull base, prostate, lung and breast cancer outnumber the other malignancies (Laigle-Dondey et al. 2005; Layer et al. 1999).

5.2 Mimics of Malignant Lesions Causing Diffuse or Multi-focal Skull Base Involvement

Diffuse replacement of the fatty bone marrow by red bone marrow due to chronic anemia may mimic

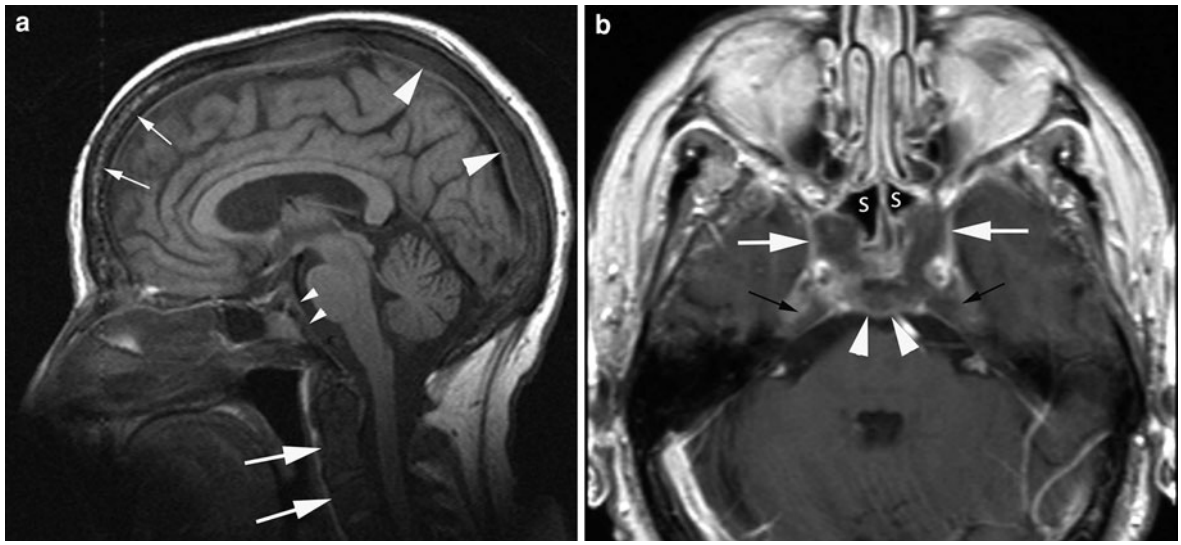

Fig. 8 Sagittal, non-contrast enhanced T1-weighted image (**a**) demonstrates completely replaced fatty bone marrow by diffuse metastatic disease in the majority of the skull (*large arrowheads* in **a**) and cervical spine (*large arrows* in **a**) while the bone marrow of the frontal skull is more mottled in appearance (*small arrows* in **a**) that is consistent with less extensive involvement. In addition, there is lack of fatty bone marrow within the clivus (*small arrowheads* in **a**) due to involvement by metastatic disease. The extent of the skull base metastasis is markedly better seen on the axial, contrast enhanced T1-weighted image (**b**) showing posterior bulging of the clivus (*arrowheads* in **b**), extension into the petrous apex bilaterally (*black arrows* in **b**), into the cavernous sinuses (*white arrows* in **b**) and into the sphenoid sinuses (*s* in **b**)

diffuse infiltration of the skull base by an underlying malignant entity. MR imaging findings are often not helpful as both entities result in decreased intensity of the bone marrow on T1- and fast spin-echo T2 weighted images and show enhancement following intravenous contrast administration (Laigle-Dondey et al. 2005; Yildrim et al. 2005; Loevner et al. 2002). CT may or may not provide additional clues as not all patients with multiple myeloma, lymphoma, leukemia or metastatic disease show bony destruction within the diploic space or early erosions of the inner and/or outer table. Therefore, clinical history and laboratory results might provide the most helpful information in some patients. Bone marrow expansion can also occur and mimic diffuse malignant involvement of the skull base and skull. It is usually seen with severe anemia such as hemolytic anemia or thalassemia (Yildrim et al. 2005; Tunaci et al. 1999). MR might deliver ambiguous results but CT usually solves the dilemma as the bone thickening caused by the bone marrow expansion is disproportionate to the preserved diploic trabecula and the intactness of the inner and outer tables of the skull (Fig. 10). Sites of extrapoetic bone marrow, such as within the paranasal sinuses, might occasionally also be seen, supporting the benign nature of the bone marrow expansion (Tunaci et al. 1999; Joseph et al. 2004).

Gorham, or vanishing bone disease, is an extremely rare bone disorder that can occur at any age and affects both genders equally. This disease is characterized by osteolysis of unknown etiology associated with angiomatous proliferation within the bone or adjacent soft tissues (Gorham et al. 1954). It can manifest as single or multiple lytic lesions involving any bone, but the calvarium and the mandible are most commonly affected (Fig. 11). Since it is such a rare entity, metastatic disease or multiple myeloma is by far the most common cause of multiple lytic bony lesions.

5.3 Non-region Specific, Localized Malignant Skull Base Lesions

All malignancies that can cause diffuse or multi-focal involvement of the skull base (metastatic disease, lymphoma, leukemia and plasmocytoma) as well as different sarcomas can present as localized lesions anywhere in the skull base. These might be difficult to distinguish from each other without further clinical

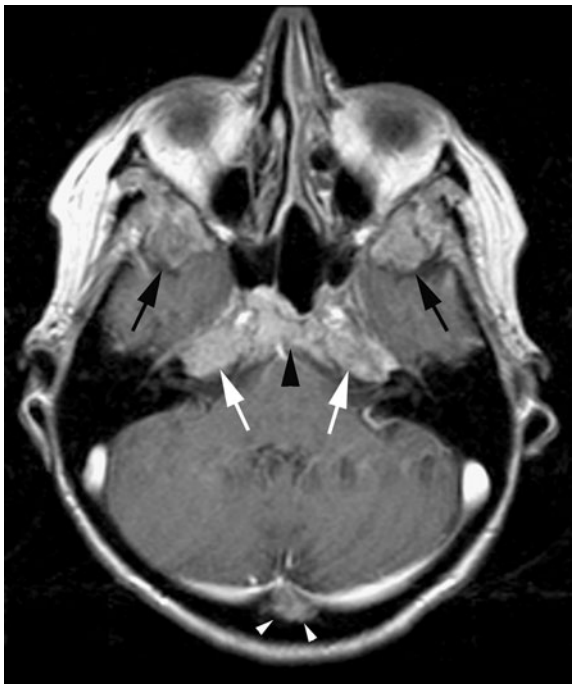

Fig. 9 Axial, contrast enhanced T1-weighted image through the upper orbit level shows replacement of the fatty bone marrow with associated bony expansion in the greater sphenoid wings bilaterally (*black arrows*), clivus (*black arrowhead*), petrous apices (*white arrows*) and in the occipital skull (*white arrowheads*) related to multiple myeloma

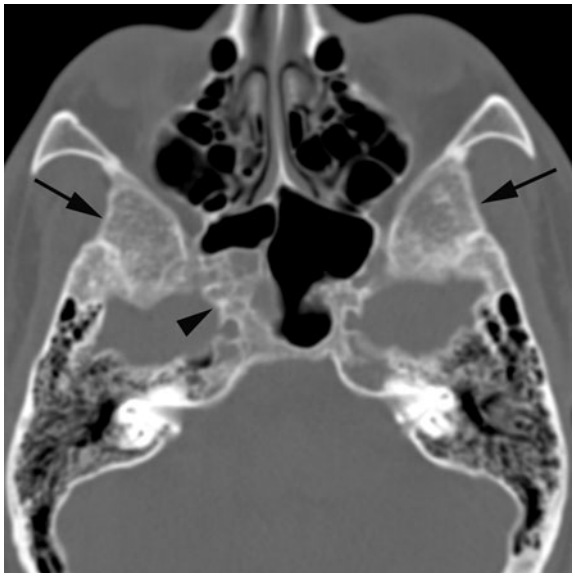

Fig. 10 Axial CT displayed in bone window demonstrates marked expansion of the greater sphenoid wings (*arrows*) that is also more cystic in appearance within the body of the sphenoid bone on the right (*arrowhead*). Thalassemia is the underlying cause of bony expansion in this patient

information. In general, metastatic disease is more aggressive in appearance and causes frank bone destruction even in early stages, while localized lymphoma and leukemia (often referred to as chloroma) show more permeative growth pattern with preservation of the diploic trabecula and of the cortical bony margins even with large tumors (Figs. 12, 13). In addition, it has been reported that highly cellular tumors with small extracellular compartment, such as lymphoma, leukemia and Ewing' sarcoma, often demonstrate pronounced restricted diffusion on the diffusion weighted images (DWI), with increased signal intensity on the DWI and reduced signal intensity on the apparent diffusion coefficient (ADC) maps (Guo et al. 2002; Mascalchi et al. 2005). In contrast, metastatic disease shows markedly less frequently restricted diffusion. Therefore, DWI might be a useful tool in narrowing the differential diagnostic possibilities in patients with inconclusive conventional MR and clinical findings.

Ewing's sarcoma is a rare and highly malignant neoplasm of the bone arising from the primitive neuroectoderm (Rueda-Franco and Lopez-Correla 1995; Kozlowski et al. 1991). It most commonly involves the long bones, pelvis, ribs and only very rarely the skull base and vault. It typically occurs in children between 5 and 13 years of age. Neurological deficits are the leading clinical symptoms caused by the mass effect from the tumor. Aggressive chemotherapy is the primary and usually successful treatment choice for Ewing's sarcoma, while surgery is reserved for cranial nerve decompression and radiation therapy for tumors unresponsive to chemotherapy (Carlotti et al. 1999). On imaging, Ewing's sarcoma presents as an osteolytic lesion causing erosions of the inner and/or outer table in association with an extracranial soft tissue mass of variable size and a significant epidural component causing local mass effect upon the adjacent brain parenchyma. The epidural component of the tumor rarely invades the dura or the brain parenchyma. On CT, the tumor itself is usually iso- to hyperdense and shows heterogeneous enhancement following intravenous contrast administration. MR is superior in delineation of the epidural component to adjacent dura and brain parenchyma. In addition, the restricted diffusion seen on the DWI part of the study might provide useful hints to the nature of the mass (Guo et al. 2002; Mascalchi et al. 2005).

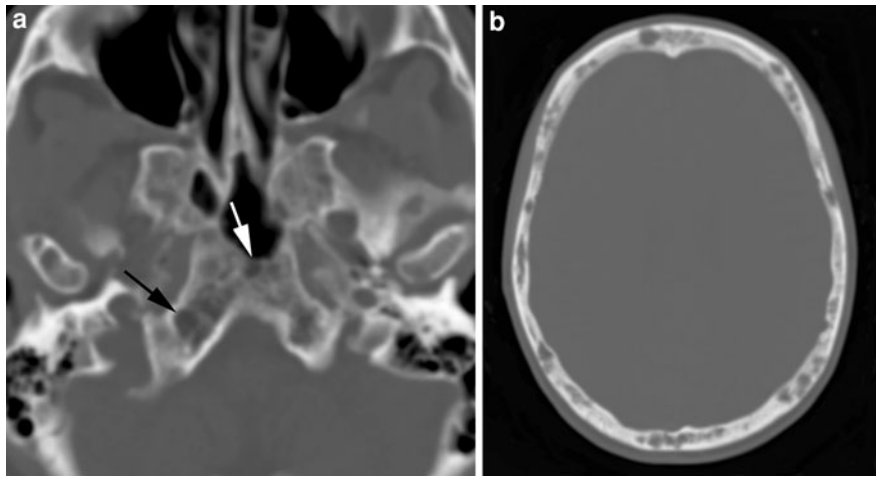

Fig. 11 Axial CT images displayed in bone window through the central skull base (**a**) and skull (**b**) show multiple small pounched out skull base (*arrows* in **a**) and numerous skull lesions caused by Gorham's disease

Fig. 12 Axial CT image displayed in bone window shows destruction of the sphenoid body (*arrowheads*) and clivus (*arrow*) caused by an aggressive skull base metastasis

Osteosarcoma is the second most common primary bone tumor after multiple myeloma of the skeleton. It typically arises from the metaphysis of the long bones, especially of the femur and proximal tibia. It only very rarely involves the skull and skull base. Secondary osteosarcomas are also rare and usually occur in the setting of previous radiation therapy or arise from benign lesions with malignant potential such as Paget's disease, multiple osteochondromatosis and chronic osteomyelitis (Salvati et al. 1993; Shinoda et al. 1993). The imaging characteristics depend on the type of the osteosarcoma. While parosteal osteosarcoma is limited to the outer table, the other types of osteosarcomas show inner and outer table involvement with associated involvement of the subdural space and brain parenchyma in approximately 40% of cases (Garland 1945). The degree of intracranial involvement is inversely related to patient's prognosis (Whitehead et al. 1998). Small fluid–fluid levels may be seen in cases of telangiectatic osteosarcoma. Radical surgical excision is the treatment of choice which is usually not feasible in the skull base. Therefore, patients with skull base osteosarcomas carry a worse prognosis than patients with osteosarcomas of other parts of the skeleton.

5.4 Mimics of Non-region Specific, Localized Malignant Skull Base Lesions

Fibrous dysplasia of the skull base is relatively common and is a developmental anomaly of the bone forming mesenchyma in which the transformation of woven to lamellar bone is disturbed. This causes an arbitrary arrangement of the bony trabeculae that are embedded in an overgrowth of a well-vascularized fibrous stroma. It represents a benign lesion, with extremely low potential for malignant transformation that usually occurs secondary to radiation therapy (Utz et al. 1989). Fibrous dysplasia is often mistaken for a skull base tumor as it can assume any appearance on MR imaging (Fig. 14; Chong and Fan 1998; Utz et al. 1989). It may show low intensity on all

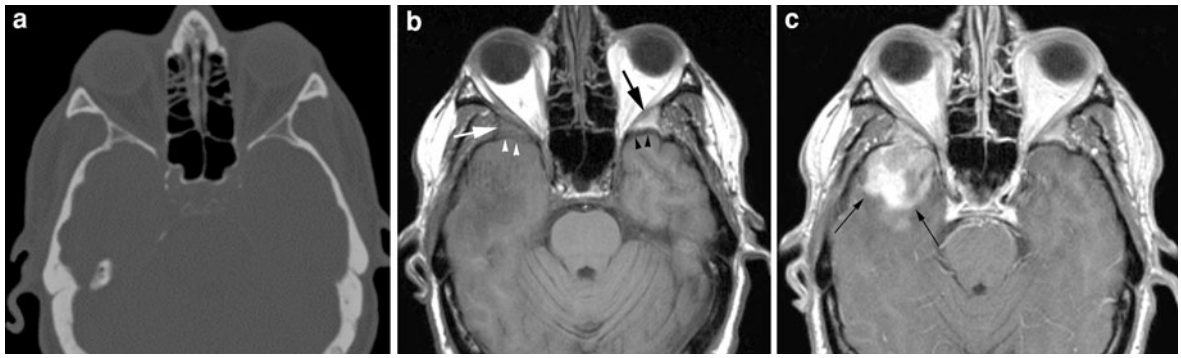

Fig. 13 Axial CT image displayed in bone window (**a**) demonstrates normal appearance of the greater sphenoid wings bilaterally. On the non-contrast enhanced T1-weighted image (**b**) diffuse infiltration of the bone marrow within the right greater sphenoid wing (*white arrow* in **b**) is noted when compared to its normal appearance on the left (*black arrow* in **b**) that is obscured on the post-contrast enhanced T1 weighted image (**c**). Also notice that the posterior cortex of the greater sphenoid wing on the left is markedly thicker in appearance (*black arrowheads* in **b**) than on the right (*white arrowheads* in **b**). The contrast-enhanced T1 weighted image (**c**) also shows the gross extension of the greater sphenoid wing mass into the middle cranial fossa and the brain invasion (*arrows* in **c**). The discrepancy of the imaging findings between CT and MR in regard to bone involvement is characteristic of lymphoma—the diagnosis in this patient

sequences reflecting the high degree of mineralization but can also demonstrate any other combination of signal intensities on the various sequences, without or with mild to extensive enhancement, reflecting the different degrees of fibrous and cystic components. In contrast, plain radiographs and CT show characteristic imaging features with bone marrow expansion, "ground-glass" appearance and preservation of the adjacent cortex (Fig. 14d). Occasionally, fibrous dysplasia presents as a lytic lesion. It is usually unilateral and monostotic in nature. It can occur anywhere in the skull but prefers the anterior and central skull base. It spares the membranous labyrinth, facial nerve canal and the internal auditory canal. Clinically, it is silent in the majority of cases and is usually incidentally found on imaging. The symptomatic patients seek medical attention because of cosmetically undesirable skull and/or facial deformities, or neurological symptoms caused by narrowing of the skull base neural foramina and subsequent cranial nerve compression that may benefit from decompressive surgery.

Langerhans cell histiocytosis is a group of idiopathic neoplasms characterized by proliferation of mature eosinophilic and specialized bone marrow-derived Langerhans cells. Three major types have been described based on clinical course: acute, fulminant, disseminated form (Letterer–Siwe disease), intermediate form (Hand–Schüller–Christian disease) and indolent/chronic form (eosinophilic granuloma) (Satter and High 2008). Eosinophilic granuloma represents the localized form of Langerhans cell histocytosis and is the variety most commonly seen by radiologists. It typically occurs in children between 5 and 15 years of age (Howarth et al. 1999). The lesions are usually asymptomatic but may manifest with bone pain, palpable soft tissue mass or symptoms related to mass effect such as proptosis or cranial nerve neuropathies (Miller et al. 1978). Usually eosinophilic granuloma presents as unifocal bony lesions, typically involving the frontal and temporal bones (DiNardo and Wetmore 1989). On imaging, eosinophilic granuloma presents as a radiolucent, round to oval punch-out bony defect without sclerosis of its margins, with an enhancing soft tissue mass within the bony defect. Hand–Schüller–Christian disease is a chronic, systemic and multi-focal variant of Langerhans cell histiocytosis with peak onset between 2 and 10 years of age. These patients typically present with diabetes insipidus, exophthalmos, chronic otorrhea and hearing loss related to multi-focal and/or bilateral skull and skull base involvement. Other organs (lymph nodes in 50%, liver in 20%, spleen in 30%) and skin may also be involved (Howarth et al. 1999). Letterer–Siwe disease is a diffuse, systemic and most severe form of Langerhans cell histocytosis. It presents in children less than 2 years of age with skin eruption, anemia and hepatosplenomegaly. It is universally fatal within

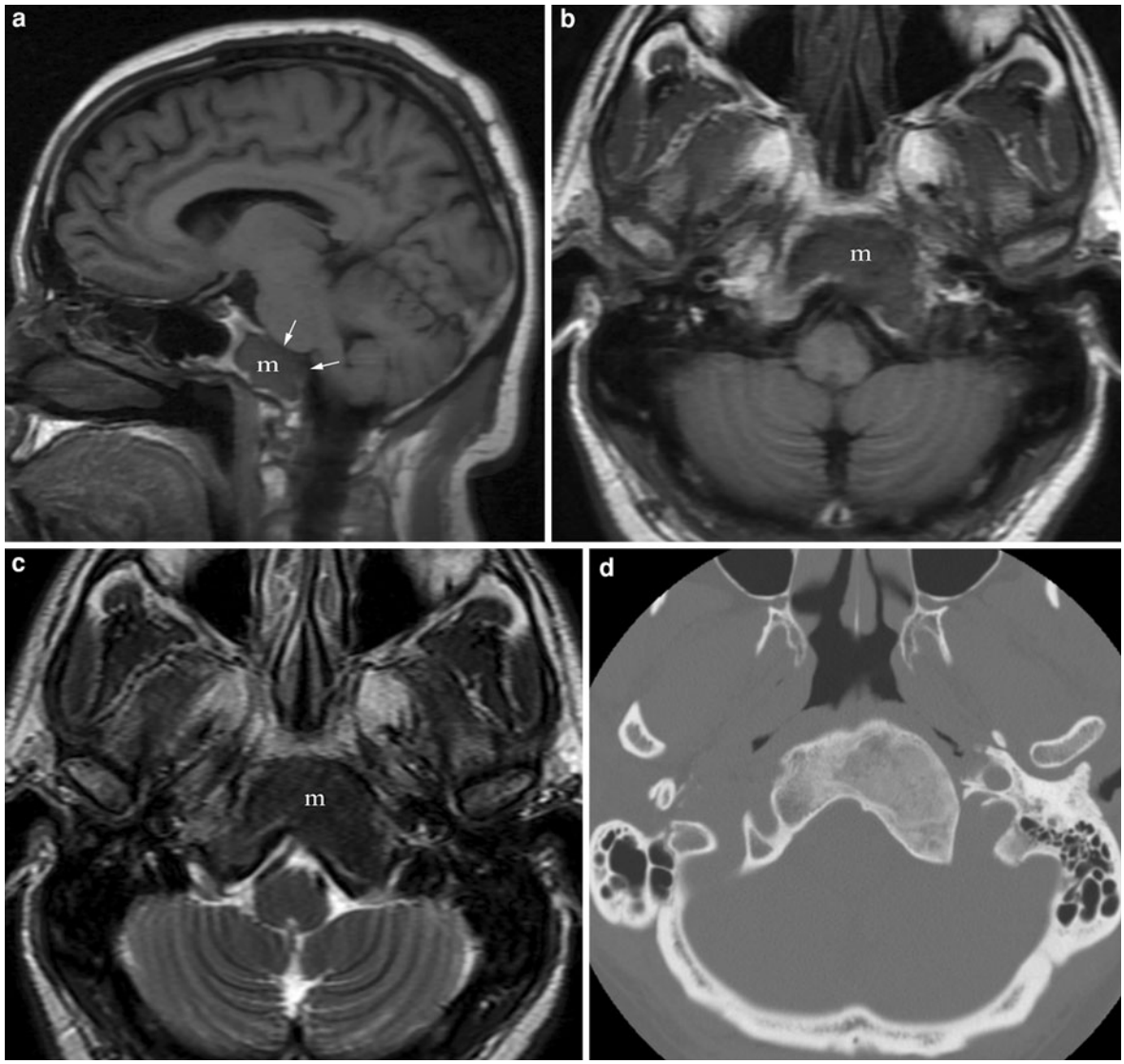

Fig. 14 Sagittal T1-weighted image through the head (**a**) demonstrates markedly abnormal bone marrow signal within the clivus (*m* in **a**) with disruption of the posterior cortex and extension into the posterior fossa (*arrows* in **a**) that is concerning for metastatic disease. The axial T1- (**b**) and T2-weighted (**c**) images through the mid clivus reveal that the lesion (*m* in **b** and **c**) is rather markedly expansile than destructive in nature and of very low signal intensity on the T2-weighted images (*m* in **b**) suggesting a benign fibrous tumor. The benign nature of the lesion was confirmed with CT (**d**) that better illustrates the expansile growth pattern and underlying ground-glass opacification characteristic for fibrous dysplasia

few years. While solitary bone lesions are treated locally with curettage or excision, systemic chemotherapy and/or bone marrow transplantation is indicated in the systemic forms of the disease (Howarth et al. 1999).

Dermoid tumors are uncommon lesions and represent inclusion cysts rather than true neoplasms. They derive from misplaced ectodermal elements during the process of neural tube closure. The tumors are usually well-defined and multi-lobulated in appearance. They have an outer connective tissue capsule lined with stratified squamous epithelium and contain hair follicles, different glands, desquamated epithelial keratin and most importantly some lipid material. This composition influences the heterogeneous appearance of these tumors on imaging.

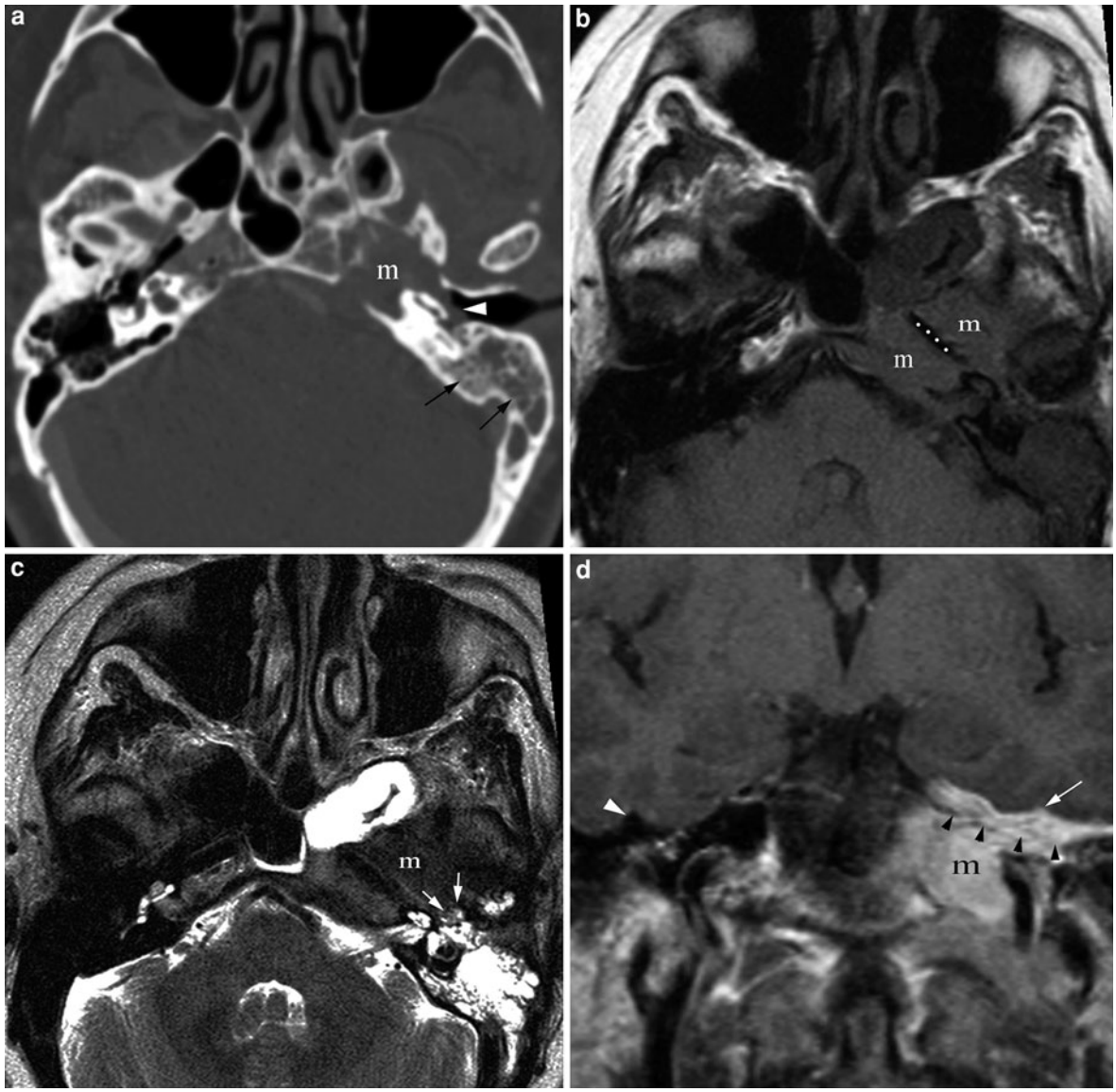

Fig. 15 Axial CT image (**a**) at the level of the sphenoid sinus incidentially discovered a destructive lesion *(m* in **a**) in the left petrous apex causing obstructive changes in the mastoid air cells (*arrows* in **a**) and complete opacification of the middle ear cavity (*arrowhead* in **a**) that could be related to direct involvement or obstructive changes. The axial T1-weighted image (**b**) reveals that the lesion (*m* in **b**) is completely surrounding the internal carotid artery (*dotted line* in **b**) within the petrous canal while the T2-weighted image (**c**) is better able to demarcate the boundary (*arrows* in **c**) between lesion (*m* in **c**) and obstructive changes within the middle ear cavity. The Gadolinium enhanced, coronal T1-weighted image (**d**) shows the superior extension of the lesion (*m* in **d**) with thick plate-like involvement of the dura *(black arrowheads* in **d**) and early invagination into the sulci of the inferior temporal lobe (*arrow* in **d**) when compared to their normal appearance on the right (*white arrowhead* in **d**). Biopsy revealed inflammatory pseudotumor rather than the initially suspected metastatic lesion

Nevertheless, these tumors typically contain various amounts of lipid material visible on imaging as very low density on CT images and high signal intensity on T1-weighted images, facilitating the correct diagnosis (Smirniotopoulos and Chiechi 1995; Gormley et al. 1994). Contrast enhancement is uncommon. Dermoid tumors involving the central nerves system typically present as a midline intracranial mass. Skull, skull

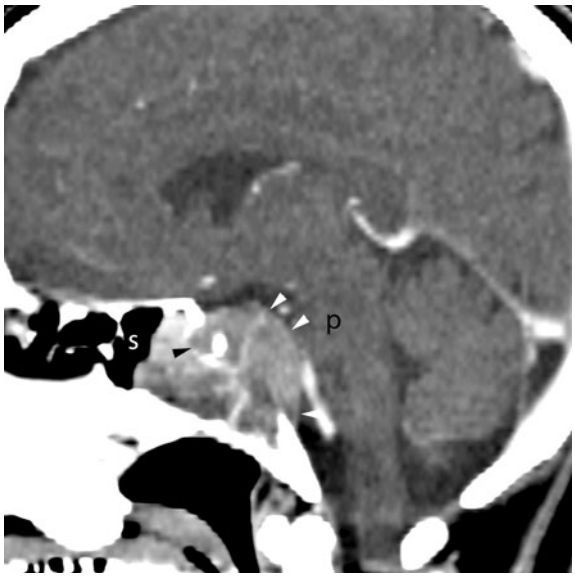

Fig. 16 Contrast enhanced, sagittal multi-planar CT reformation displayed in soft tissue window illustrates a large central skull base mass with gross invasion of the sphenoid sinus (*s*). In addition, the clivus (*c*) is almost completely involved by this mass that also bulges posteriorly into the prepontine cistern (*white arrowheads*) where it flattens the pons (*p*). The sella (*black arrowhead*) is also involved without significant suprasellar component. This represented an invasive pituitary gland adenoma. Notice the discrepancy between the suprasellar and the intraclival component that is more characteristic of aggressive pituitary gland tumor variants

base and orbit represent the most common extracranial locations of dermoid tumors in the head and neck region (Cummings et al. 2004). Complete surgical excision is the standard treatment. Resectability, however, depends upon the location of the tumor, e.g. encroachment upon vasculature and nerves.

Inflammatory pseudotumors of the skull base are rare. They represent idiopathic, non-neoplastic lesions that typically show locally aggressive behavior and marked enhancement mimicking malignant skull base neoplasm (Fig. 15; Garg et al. 2010). No specific imaging features have been reported and therefore, the diagnosis can only be made by biopsy and/or resection. Proliferation of the fibroblasts with intermixed inflammatory cells is seen on pathological evaluation. Surgical resection and/or corticosteroid administration are usually the treatment option of first choice, with radiation therapy reserved for recurrent disease (Williamson et al. 2003).

5.5 Malignant Central Skull Base Lesions

Invasive and malignant pituitary gland tumors are rare and represent a continuum of disease, as pituitary carcinomas usually occur in the setting of pre-existing invasive pituitary gland tumors (Ragel and Couldwell 2004). Both show locally aggressive growth pattern with tendency for early skull base invasion, in contrast to the slowly growing benign pituitary gland tumors that like to decompress into the suprasellar cistern (Fig. 16). Distinct immunohistochemical markers (interleukin 6 and heat shock protein 27) that have been found to be elevated in invasive types but not in the benign variants of pituitary gland tumors are thought to be responsible for this biological aggressiveness of the invasive tumor variants (Gandour-Edwards et al. 1995). Often these tumors are large at presentation or fast growing on serial follow-up. Otherwise, they show similar imaging characteristics to their benign variants. Their large size and local aggressive growth pattern sometimes make them difficult to distinguish from other malignant central skull base lesions (Figs. 16, 17). The majority of invasive variants of pituitary gland tumors are endocrinologically active with 42% secreting adrenocorticotrophic hormone (ACTH) and 33% prolactin. The presence of metastatic disease distinguishes the invasive pituitary gland tumor from the carcinoma form (Ragel and Couldwell 2004). Metastatic disease primarily occurs in the central nervous system (cerebrum, cerebellum, spinal cord, leptomeninges and subarachnoid space) and search for it needs to be conducted in suspected invasive pituitary gland tumor as metastatic lesions might be already present on the initial imaging study. Systemic metastases most commonly involve lymph nodes, bone, liver and ovaries. Overall, pituitary carcinomas have a very poor prognosis with a reported 1-year survival rate of 34%. For the patient it is critical that the radiologist recognizes the invasive nature of a pituitary gland tumor, as an aggressive treatment plan is critical prior to development of metastatic disease.

Neuroblastoma is an embryonal malignancy arising from neuroblasts of the sympathetic nervous system (Brodeur and Castleberry 2001). They can occur as primary or secondary neuroblastomas of the skull base. The primary neuroblastomas arise from the olfactory bulb and are discussed in

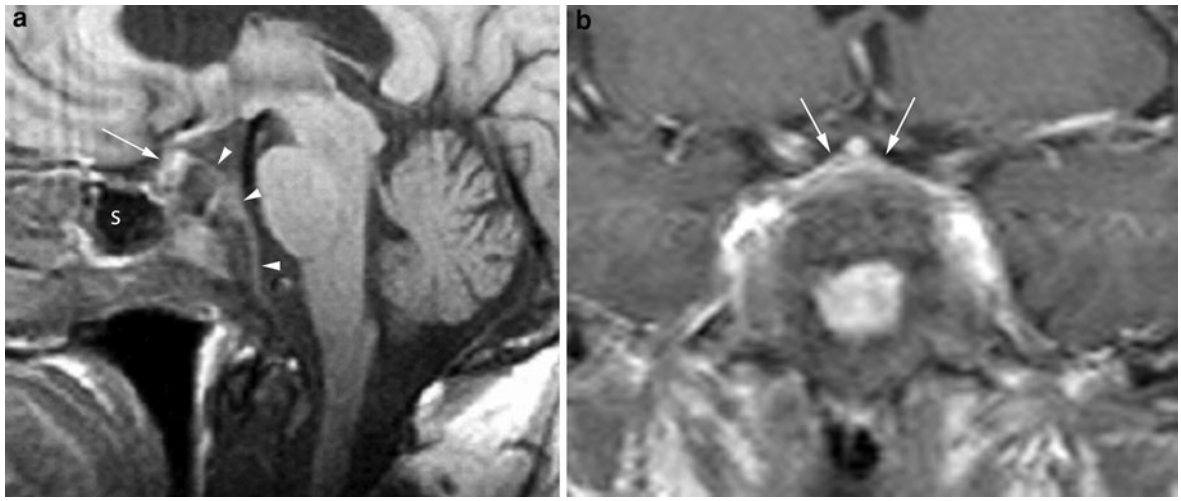

Fig. 17 Sagittal (**a**) and coronal (**b**) contrast enhanced T1-weighted images demonstrate a large central skull base mass completely involving the clivus. The extent of the mass is similar to Fig. 16 although the sphenoid sinus (*s* in **a**) is not involved and the posterior bulging into the prepontine cistern (*arrowheads* in **a**) is not as extensive. More important, however, is that the pituitary gland can be seen as it is displaced anterior and superior on the sagittal view (*arrow* in **a**) and is markedly flattened on the coronal view (*arrows* in **b**) obviating an invasive pituitary tumor as the etiology of this skull base mass. This represented a metastatic lesion

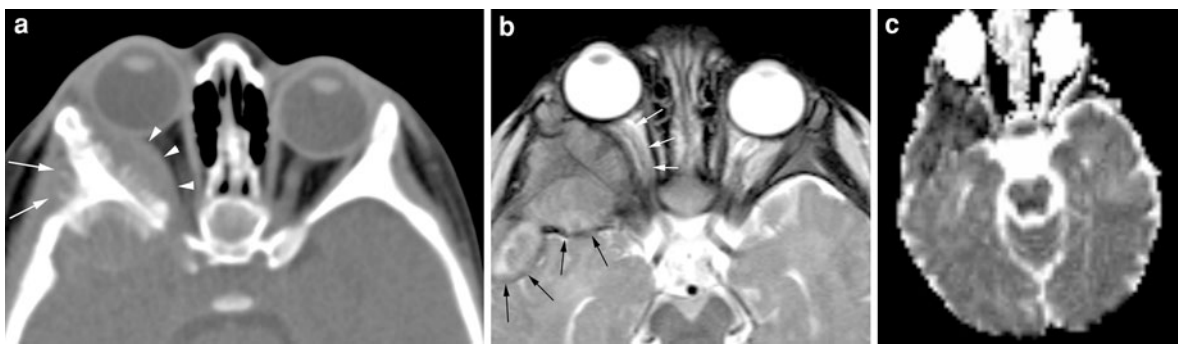

Fig. 18 Axial CT image displayed in soft tissue window (**a**) shows a large mass centered in the greater sphenoid wing on the right side (*arrows* in **a**) with extensive periosteal reaction and an orbital component (*arrowheads* in **a**). The intracranial component (*black arrows* in **b**) is markedly better seen on the axial T2-weighted image (**b**) that also displays the displacement of the optic nerve sheath complex medially (*white arrows* in **b**). The ADC map (**c**) shows lower attenuation than the adjacent brain parenchyma consistent with restricted diffusion that is characteristic of small blue cell tumors such as neuroblastoma metastasis

"Neoplasms of the Sinonasal Cavities". Secondary neuroblastomas represent metastatic disease to the skull base with a tendency for orbital wall involvement including the portions formed by the greater sphenoid wings (Fig. 18). Little has been reported in regard to imaging findings of metastatic neuroblastoma to the skull base, however, since neuroblastoma is a small cell tumor with high cellularity and little extracellular space it is not surprising that it shows restricted diffusion on DWI (Fig. 18c). Patients with orbital involvement may present with proptosis, periorbital ecchymosis, diplopia or vision loss. Otherwise, the symptoms are related to the primary lesions, "blueberry muffin" resembling skin disease or a paraneoplastic systemic syndrome with myoclonic jerking and random eye movements (=opsoclonus) (Brodeur and Castleberry 2001). The treatment and prognosis of neuroblastoma depends upon tumor stage, age of the patient, histological and molecular features.

In the central skull base region, schwannomas may arise from cranial nerve III–VI. Benign trigeminal nerve (cranial nerve V) schwannomas are the most

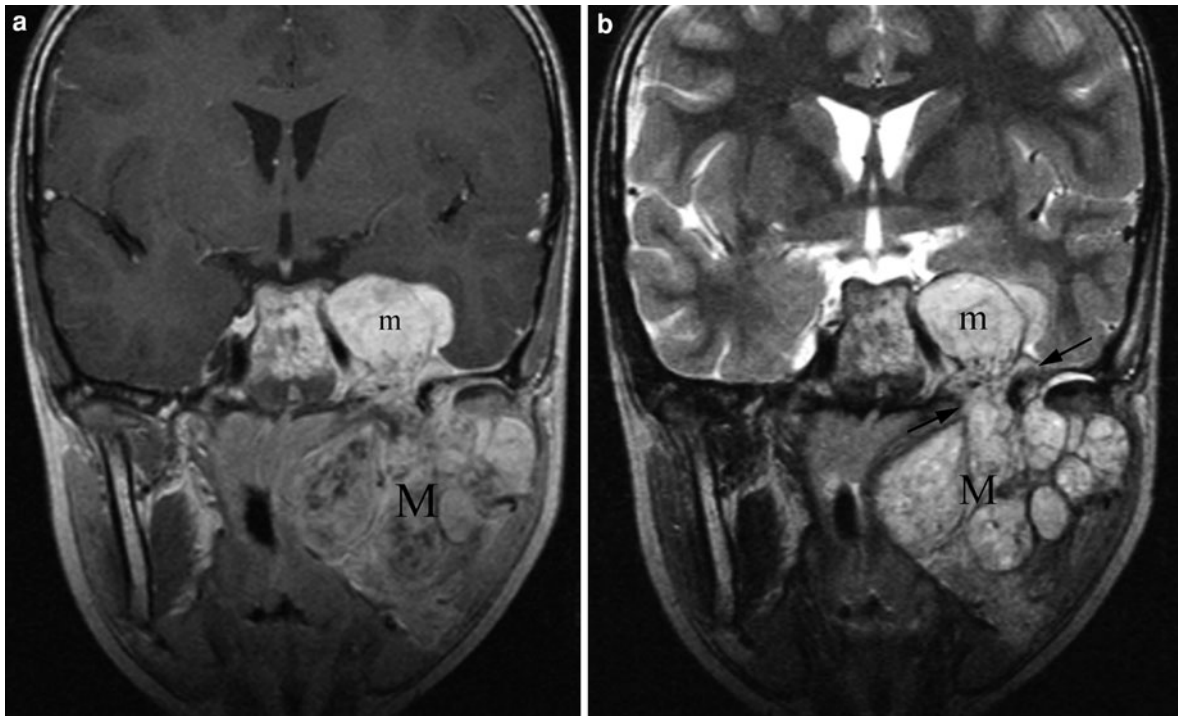

Fig. 19 Gadolinium enhanced, coronal T1- (**a**) and T2-weighted (**b**) images through the central skull base show a large, markedly enhancing left cavernous sinus mass on the left (*m* in **a** and **b**) that extends through the foramen ovale (*arrows* in **b**) along the mandibular division of the trigeminal nerve to completely occupy the infratemoral fossa (*M* in **a** and **b**). The very large size of the neuronal tumor in a patient without neurofibromatosis has to raise the concern for a malignant variant, requiring more aggressive treatment, as was the case in this patient

common cranial nerve tumors with a reported incidence of up to 0.4% of all intracranial tumors. Malignant schwannomas are even more rare. All but trigeminal nerve malignant schwannomas have been linked to neurofibromatosis type 1 (Stone et al. 2001). Malignant schwannomas of the trigeminal nerve are rather sporadic in occurrence with no known risk factors. The clinical presentation of the benign and malignant variants of central skull base schwannomas is similar, related to dysfunction of the cranial nerve primarily involved and mass effect-related dysfunction of the remaining cranial nerves within the cavernous sinuses. There are no characteristic imaging features distinguishing between benign and malignant types of schwannomas either. The more aggressive nature of the schwannoma may be suggested when rapid tumor growth or extensive nerve involvement is seen (Fig. 19). In addition, presence of early erosions of the skull base foramina that are disproportionate to the size of the schwannoma might provide important clues (Stone et al. 2001). Due to the rarity of malignant schwannomas little is known in regard to most optimal treatments. Complete surgical resection is certainly the main goal but usually not feasible. In addition, it has been reported that malignant schwannomas have 50% local recurrence rate despite negative surgical margins and adjuvant radiotherapy (Jabre et al. 2000). Therefore, the overall prognosis is poor with a reported 5-year survival between 38 and 65% (Stone et al. 2001).

Primary extra-dural meningioma of the skull base is rare with its malignant variant being extraordinarily uncommon (Van Tassel et al. 1991). Both entities will be discussed in this section together as their imaging findings overlap and the benign form may mimic malignant central skull base lesions. Primary extra-dural meningiomas are thought to arise from ectopic meningocystes or arachnoid cap cells that are trapped in a fracture line or suture during trauma or molding of the head at birth, respectively (Turner and Laird 1966; Azar-Kian et al. 1974). Most commonly extra-dural meningiomas are therefore intra-osseous in

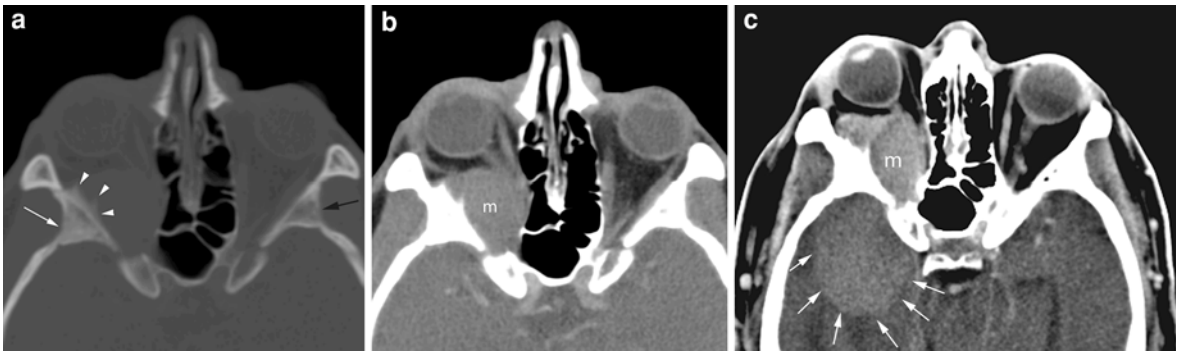

Fig. 20 Axial CT images displayed in bone (**a**) and soft tissue (**b**) windows show slight sclerosis of the greater sphenoid wing on the right (*white arrow* in **a**) when compared to the left (*black arrow* in **a**) with marked periosteal region (*arrowheads* in **a**) and a large orbital component (*m* in **b**) causing mild proptosis. These CT findings and mass location are typical of an extra-dural, intra-osseous meningioma. Axial contrast-enhanced CT image of the same patient performed 6 months later (**c**) shows moderate enlargement of the orbital component (*m* in **b**) with more pronounced protosis and a new large intracranial component (*arrows* in **c**) that extended superiorly to involve the lower half of the frontal lobe (not demonstrated). The rapid growth pattern of this mass is consistent with a malignant meningioma that was confirmed surgically and on pathological evaluation

nature and often involve the greater sphenoid wing which is in part related to the high number of sutures in this location (Fig. 20). In contrast to the intradural variant, there is no gender preference and the extra-dural type shows a bimodal peak with manifestation at older age as well as in the second decade of life (Lang et al. 2000). More than half of these lesions are hyperostotic on plain films and CT studies potentially mimicking prostatic cancer metastasis or fibrous dysplasia (Fig. 20a). Only approximately 35% present as osteolytic and 6% mixed lesions (Crawford et al. 1995; Tokgoz et al. 2005). Spiculated appearing periosteal reaction might be present (Fig. 20a). Often a soft tissue component of variable size is seen which might be difficult to distinguish from adjacent musculature and/or dura on CT images (Fig. 20b, c). MR is superior in this regard due to its increased soft tissue detail. As on CT, extra-dural meningiomas may show variable internal signal characteristics and different degrees of contrast enhancement primarily reflecting the degree of hyperostosis. Interestingly, it has been shown that the extra-dural type of meningiomas has a higher incidence of malignant degeneration than the intradural variant with a reported risk of 11 and 2%, respectively (Tokgoz et al. 2005). It has been described that meningiomas presenting with osteolysis and an extracranial soft tissue component are more likely aggressive, and therefore, more often malignant in nature (Fig. 20). In addition, it has been shown that malignant meningiomas have the tendency to show restricted diffusion on DWI (Fillippi et al. 2001). Complete surgical resection is the treatment of first choice.

5.6 Mimics of Malignant Central Skull Base Lesions

Cephalocele is a rare entity, in which brain tissue and/or meninges are protruding through a bony defect from intracranial to extracranial. In the central skull base region, intra-sphenoidal and trans-sphenoidal cephaloceles have been encountered (Jabre et al. 2000). Trans-sphenoidal cephaloceles are usually congenital in nature. They are typically midline in position and therefore may present on imaging as a midline bony gap associated with a cystic nasopharyngeal mass. This type of cephalocele is usually complex in nature containing optic nerves, hypothalamus or other adjacent midline structures. These patients might present with pituitary gland dysfunction due to protrusion of the pituitary gland into the meningoencephalocele or more commonly because of associated maldevelopment of the sella and pituitary gland. The intra-sphenoidal cephaloceles are typically lateral in location and most commonly post-traumatic in nature. These usually contain variable amounts of temporal lobe tissue and may present with seizures or rhinorrhea, bearing increased risk of meningitis. Therefore, they are often treated with surgery. On CT,

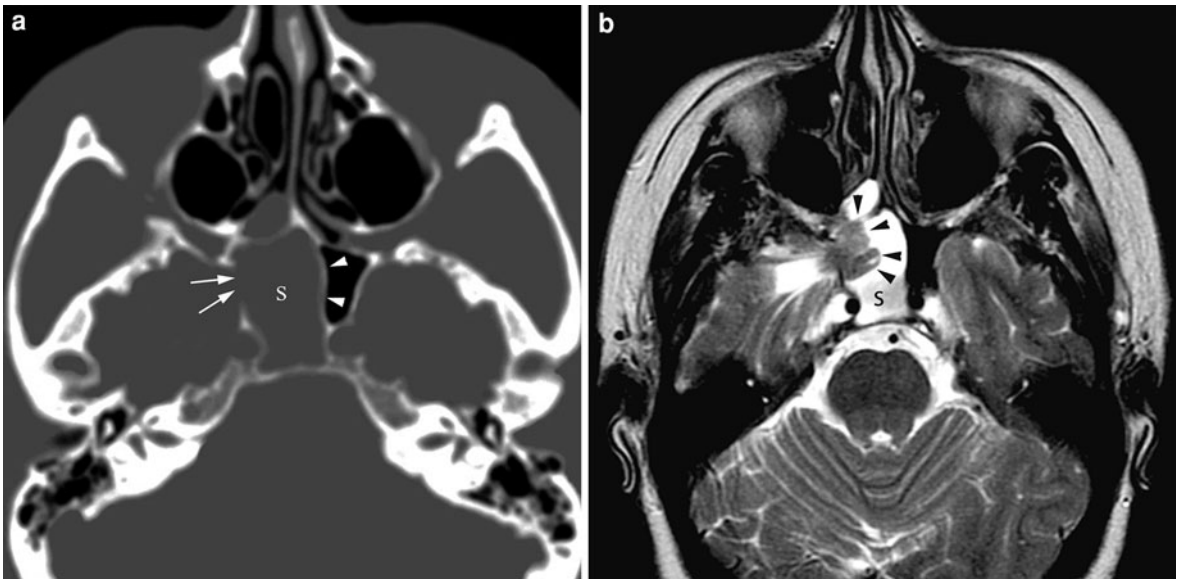

Fig. 21 Axial CT image displayed in bone window (**a**) demonstrates complete opacification of the sphenoid sinus on the right (*s*) with an approximately 1-cm bony gap in the lateral wall of the sphenoid sinus (*arrows* in **a**) and mild bowing of the sphenoid septum to the left (*arrowheads* in **a**). Although these imaging findings might be mistaken for a sphenoidal mucocele and less likely for an aggressive sphenoid sinus tumor, the direction of bowing of the edges of the bony gap suggests that this is an intracranial process secondary involving the sphenoid sinus. This is confirmed on the axial T2-weighed image (**b**) that clearly shows protrusion of brain tissue (*arrowheads* in **b**) into the sphenoid sinus (*s* in **b**) through the bony defect. These imaging findings are therefore consistent with a lateral intrasphenoidal encephalocele

a bony gap in the sphenoid body and partial or complete opacification of one or both sphenoid sinuses is seen (Bolger and Reger 2003). They may be mistaken for mucoceles or aggressive skull base masses when associated with mass effect within the sphenoid sinus (Fig. 21a). On MR the diagnosis is easier as the extracranial brain tissue and/or meninges are directly demonstrated in particular on T2-weighted images (Fig. 21). On CT, however, the location of the bony gap, the pattern of bone remodeling rather than destruction and potentially associated mild bowing of the involved bone towards the sphenoid sinus provide important diagnostic clues that warrant further evaluation with MRI.

5.7 Malignant Lesions at the Junction of Central to Posterior Skull Base

Chordomas represent rare, locally invasive and slowly growing tumors. Histologically, they resemble benign tumors, however, the majority of authors consider them as low grade malignancies due to their aggressive local growth pattern and their low risk for metastatic disease (Erden et al. 2003). They originate from embryonic remnants of primitive notochord at the spheno-occipital synchondrosis. The skull base is the second most common location. The majority of chondromas occur at the distal end of the notochord in the sacral region. Different histological subtypes have been reported such as chondroid and myxoid variants. Chordomas may present at any age but show a predilection for the fourth decade and males. The onset of symptoms is insidious, reflecting the slow growth pattern of these tumors. However, at some point these patients become symptomatic and most commonly present with headaches and diplopia secondary to cranial nerve VI palsy. This is not unexpected as the cranial nerve VI courses through the medial portion of the petrous apex within Dorello's canal, in close proximity to the spheno-occipital fissure. The vast majority of chordomas are midline in position with relative symmetric bilateral tumor growth. Only less than 15% of chordomas have been reported to originate from the petrous apex simulating a chondrosarcoma. On CT, chordomas classically present as large, relatively well-circumscribed, lytic bone lesions arising from the clivus (Fig. 22a). Often intra-tumoral

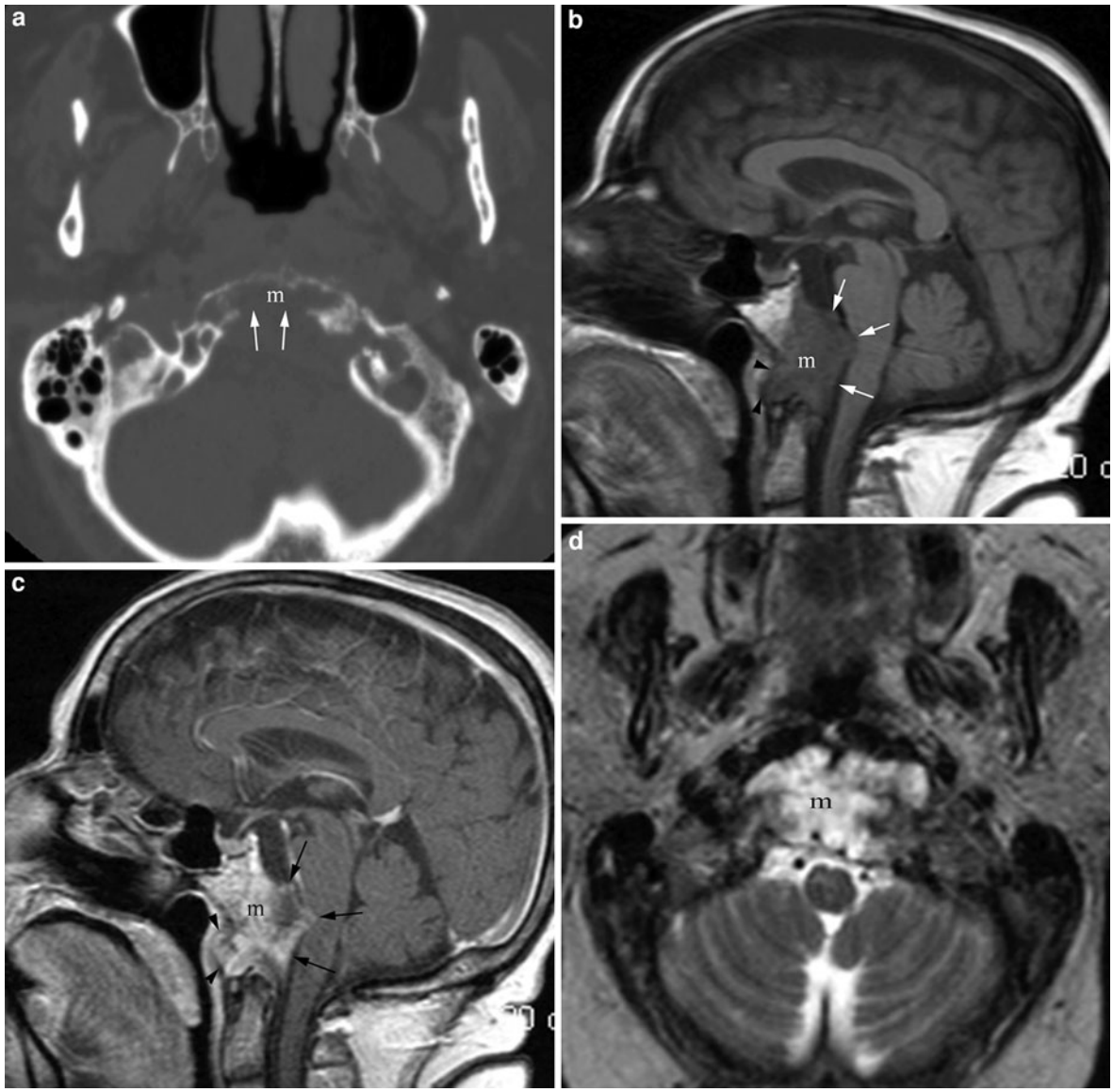

Fig. 22 Axial CT image displayed in bone window (**a**) demonstrates a moderate lytic clival mass (*m* in **a**) with complete posterior cortical disruption (*arrows* in **a**). The non-contrast enhanced (**b**) and contrast enhanced (**c**) T1-weighted images demonstrate the full extent of the markedly, heterogeneously enhancing lesion (*m* in **b** and **c**) with a small nasopharyngeal (*arrowheads* in **b** and **c**) and a large posterior fossa component (*arrows* in **b** and **c**). The clival origin of the lesion together with the marked hyper intensity on the axial T2-weighted (*m* in **d**) images is most consistent with chordoma which was confirmed with surgical biopsy

calcifications are seen, representing small bony sequestra left behind from bone destruction or true calcifications in case of the chondroid variant. The associated soft tissue mass is usually slightly hyperdense in appearance demonstrating moderate to marked enhancement following intravenous contrast administration. Although it is easy to detect a chordoma with CT, MR has been proven to be considerably superior in the delineation of the tumor extent, and is therefore the most pertinent study for treatment planning purposes. On MR imaging, chordomas show a low to intermediate T1 and high T2 signal intensity with small focal areas of decreased T2 intensity caused by tumoral calcifications or small

foci of intra-tumoral hemorrhage (Fig. 22a–c). Moderate to marked heterogeneous contrast enhancement is typically seen (Fig. 22b, c). Total surgical resection is the most optimal treatment but is usually not feasible. Therefore, post surgical radiation therapy is usually utilized to improve patient's prognosis, which is primarily affected by the amount of tumor tissue left behind within the surgical bed (Erden et al. 2003). Overall, the prognosis is poor with a reported 5-year survival rate of approximately 50% (Forsyth et al. 1993).

5.8 Malignant Posterior Skull Base Lesions

Chondrosarcomas are rare malignant cartilaginous tumors of variable aggressiveness (Evans et al. 1977). Their aggressiveness depends upon the tumor subtype and grade. The dedifferentiated and mesenchymal variants are more aggressive than the classic variant. The classic variant is the most common and represents a low grade chondrosarcoma. This type of chondrosarcoma shows the least aggressive growth pattern, minimal risk of metastatic disease and is often difficult to distinguish from chordomas histologically and clinically (Bourgouin et al. 1992). As with chordomas, headaches and diplopia related to cranial nerve VI palsy are the most common symptoms at presentation. However, chondrosarcomas usually occur in younger patients with a peak incidence in the second and third decades, and even more importantly they are off midline (petroclival) in location (Hassounah et al. 1985). Their paramedian location also predisposes these patients for lower cranial nerve deficits, in particular hearing loss. CT images typically demonstrate a destructive mass centered in the petrous apex with ring and arcs in it reflecting the chondroid nature of this tumor (Fig. 23a). Variable amount of soft tissue component is seen, typically isodense to the adjacent brain parenchyma, with some (but variable) enhancement following intravenous contrast administration. Chondrosarcomas have low to intermediate signal intensity on T1-, and high signal intensity on T2-weighted sequences, with variable enhancement pattern (Fig. 23b–d). As with chordomas, total surgical resection is the most desirable treatment in combination with radiation therapy if positive resection margins are present. Despite the histological and clinical similarities, the classic type of chondrosarcoma has been reported to have a better prognosis than chordomas with a 5-year survival rate of approximately 90%. This, however, is not true for the other chondrosarcoma variants (Forsyth et al. 1993; Evans et al. 1977).

Endolymphatic sac tumors are also very rare. They may occur sporadically or in association with von Hippel-Lindau disease (Luff et al. 2002). The patients typically present with hearing loss, tinnitus, vertigo and/or facial nerve dysfunction (Choyke et al. 1995). Bilateral involvement has been reported in von Hippel-Lindau disease patients. The majority of these tumors are low grade adenocarcinomas or papillary cystadenomas that are indistinguishable from each other based on imaging (Mukherji and Castillo 1996). On CT, local destruction is seen in the retrolabyrinthine petrous bone, at the aperture of the vestibular aqueduct, with characteristic intra-tumoral bone spiculi that might be associated with an enlarged vestibular aqueduct (Ragel and Couldwell 2004). The T1-weighted images demonstrate characteristic hyperintense foci within the tumor substance with extensive enhancement following intravenous contrast administration. Endovascular embolization prior to surgical resection may be required.

Paragangliomas are rare tumors of neural crest origin (Rao et al. 1999). In the posterior skull base, they are most commonly seen in the jugular fossa and are called glomus jugulare tumors. They arise from the paraganglion cells of the Jacobson or Arnold nerve which are branches of the cranial nerve IX and X, respectively (Rao et al. 1999). The majority of the paragangliomas are benign in nature. Up to 13% of glomus jugulare tumors have been reported to be malignant. Both types will be discussed in this section together as they both demonstrate with locally aggressive growth pattern making them indistinguishable from each other (Figs. 24, 25). Demographic data are not helpful either as both forms most commonly occur in middle-aged females that typically present with tinnitus (Brewis et al. 2000). It has been suggested that the incidence of pain is higher and the occurrence of hearing loss lower with the malignant variants. The main differentiating feature, however, is the existence of metastatic lesions in the malignant form (Fig. 25b). Metastatic disease most commonly spreads to the bone, lung and cervical

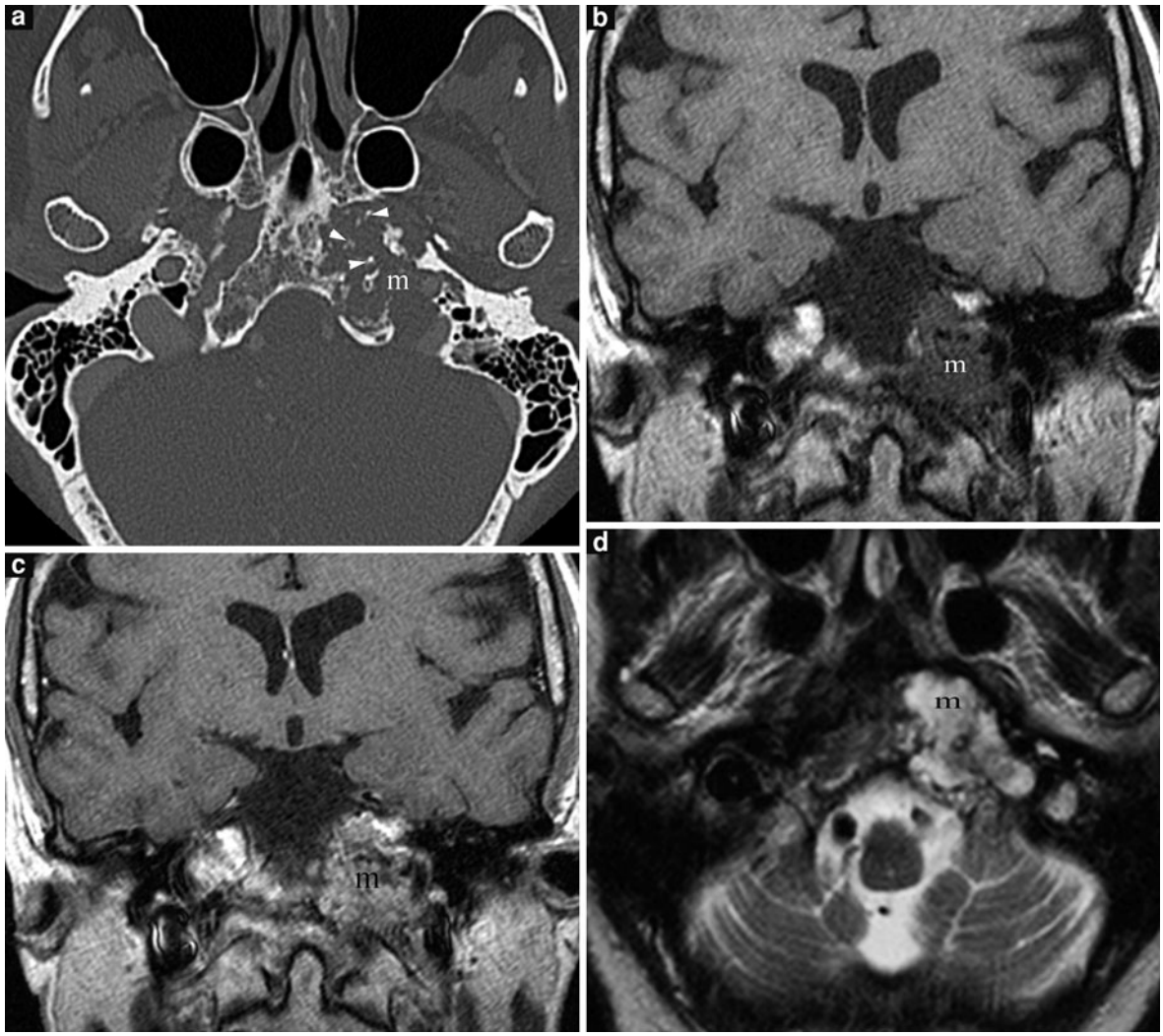

Fig. 23 Axial CT image displayed in bone window (**a**) shows a large, destructive mass (*m* in **a**) in the left petrous apex and left clivus with characteristic ring and arcs (*arrowheads* in **a**) appearance of chondrosarcomas. The MRI study confirms this suspicion by demonstrating a markedly enhancing mass in the petrous apex (*m* in **b** and **c**) on the T1-weighted images without (**b**) and with Gadolinium enhancement (**c**) with characteristic hyperintense signal intensity seen on the T2-weighted image (*m* in **d**)

lymph nodes and might present even years after the initial diagnosis and treatment (Fig. 25b). While nuclear medicine examination with Indium 111 labeled somatostatin analogs is an excellent way to evaluate for metastatic disease, CT and/or MR are primarily utilized to evaluate the primary tumor within the jugular fossa. On CT, glomus jugular tumor causes destruction of the walls of the jugular foramen and adjacent petrous bone giving the so-called "mouth eaten" appearance (Figs. 24, 25). On MR, a hypervascular mass with flow voids and extensive enhancement is seen in the jugular fossa region. On both studies, the tendency of the glomus jugulare to grow into the middle ear cavity and posterior fossa is seen, although the intracranial involvement is better demonstrated with MR (Fig. 24). In approximately 10% of patients, multifocal and/or bilateral involvement is seen. The benign forms of glomus jugulare can be treated with surgical resection following intra-arterial embolization, radiation therapy or both as the tumor is known to be radiosensitive and total surgical resection is often

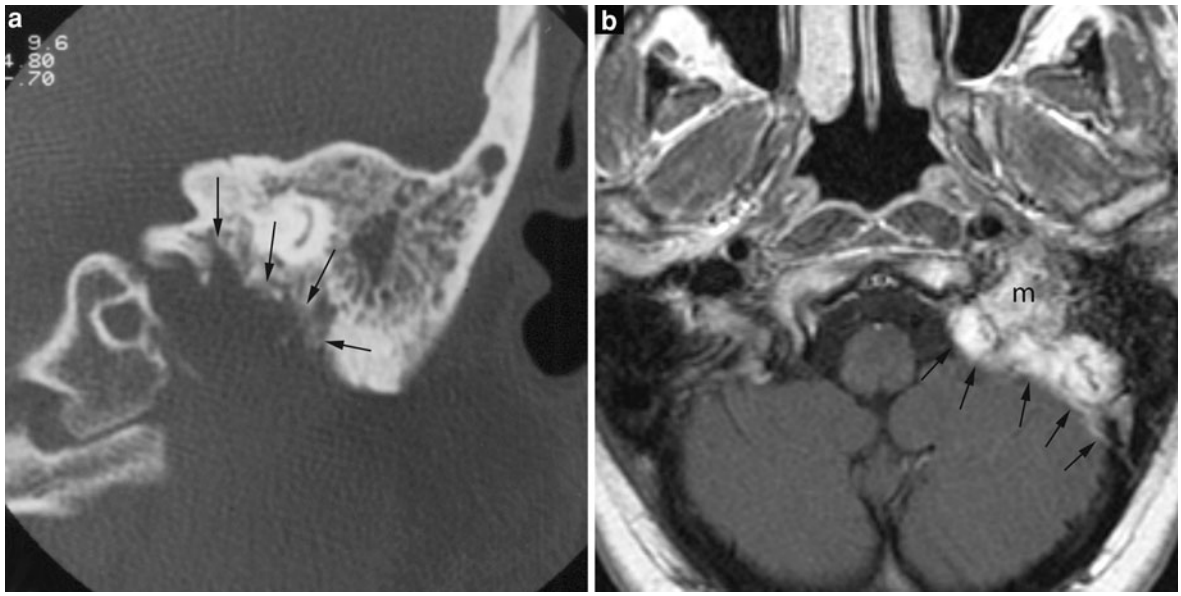

Fig. 24 Coronal CT image displayed in bone window (**a**) shows the marked erosions along the lateral and superior jugular foramen (*arrows* in **a**) caused by a large heterogeneously enhancing mass (*m* in **b**) as seen on this contrast enhanced axial T1-weighted image (**b**). The mass also extends into the posterior fossa (*arrows* in **b**) where it results in mild impression upon the left cerebellar hemisphere. The location and imaging findings are classic for a jugular foramen paraganglioma

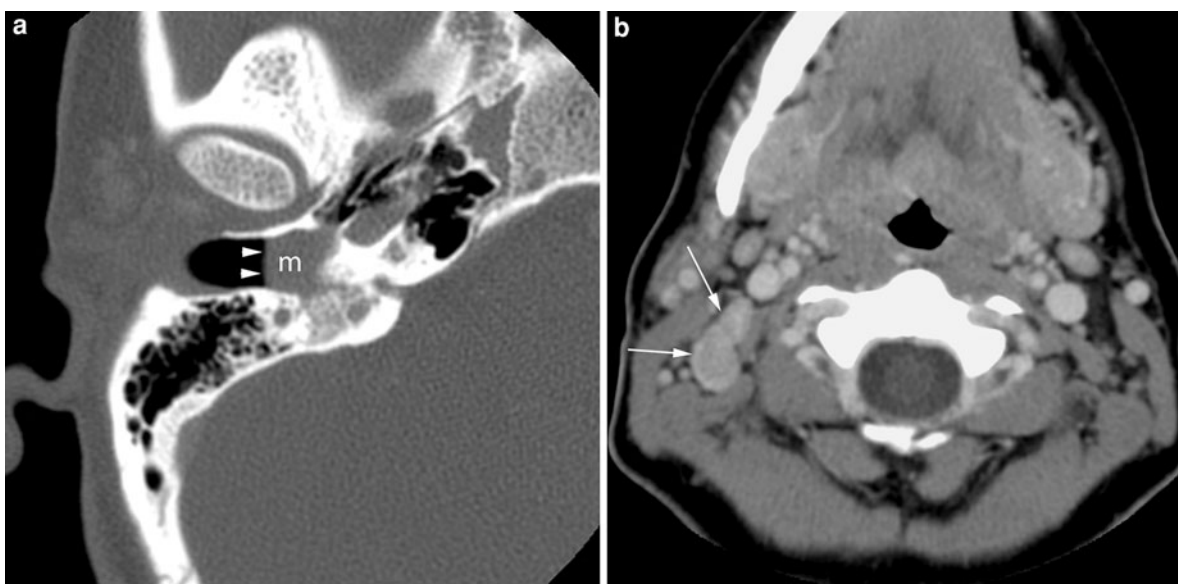

Fig. 25 Axial contrast-enhanced CT images through the middle ear displayed in bone window (**a**) and through the upper neck displayed in soft tissue window (**b**) from a 35-year-old female with tinnitus and hearing loss and with classic imaging findings of paraganglioma originating within the jugular foramen on other images. **a** Image illustrating the tendency of the jugular paragangliomas to grow into the middle ear cavity (*m* in **a**). The typpanic membrane is markedly displaced laterally (*arrowheads* in **a**). The image through the neck demonstrates abnormal group 2A lymph nodes on the right (*arrows* in **b**) allowing the diagnosis of malignant paraganglioma. This patient underwent right modified lymph node dissection confirming the nodal metastatic disease that was not suspected on clinical examination

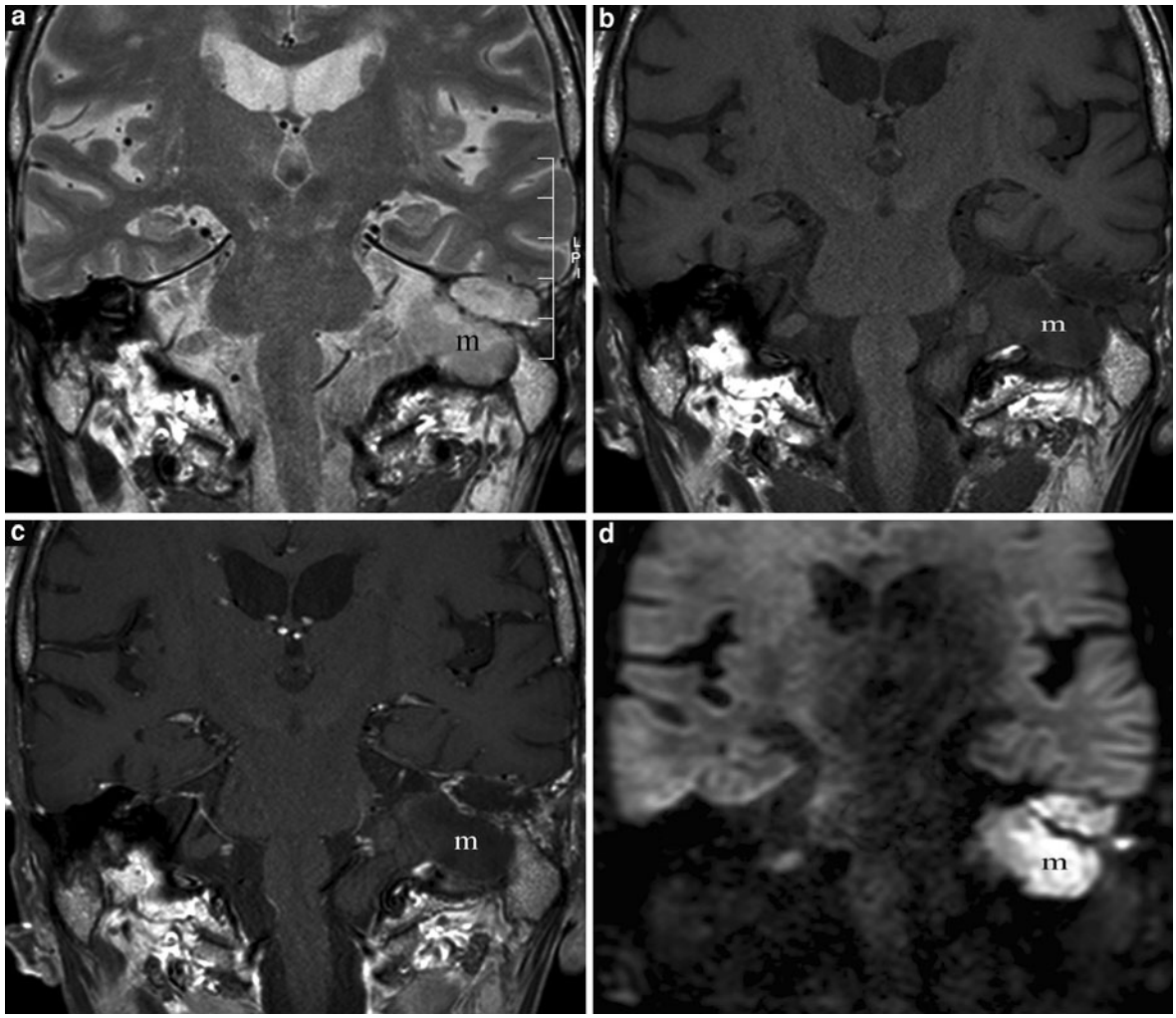

Fig. 26 Coronal T2-weighted image (**a**) demonstrates a large, hyperintense mass (*m* in **a**) in the right petrous apex region on the left side that might be mistaken for a chondrosarcoma because of its location and T2 signal intensity. The T1-weighted images pre- (**b**) and post-contrast administration (**c**), however, show lack of enhancement within the mass (*m* in **b** and **c**) which is very atypical for chondrosarcoma. In addition, the diffusion weighted image in coronal plane (**d**) shows restricted diffusion within the lesion (*m* in **d**). Cholesteatoma was confirmed on surgical specimen (Images courtesy of Robert Hermans, MD, PhD, Leuven, Belgium)

difficult. Since radiation therapy is known to leave a residual mass of variable activity behind, treatment of the malignant forms with radiation therapy alone is currently not recommended but rather surgical resection with post-operative radiation therapy. Utilization of Iodine 131 labeled MIBG for treatment of the metastatic lesions has been reported with mixed preliminary results (Bomanji et al. 2001). Paragangliomas are increasingly recognized to have a genetic predisposition, with mutations of the enzyme succinyl dehydrogenase (SDH) resulting in paraganglioma formation. Several types of mutation of this enzyme are known: SDHB mutation possibly leading to extra-adrenal pheochromocytomas, malignant paragangliomas and extra-paraganglial neoplasia; SDHD mutatation is associated with an increased incidence of multiple benign head and neck paragangliomas. Therefore, discovery of a paraganglioma should promp a genetic test in search of a possible SDH mutation (Barber et al. 2011).

Malignant schwannomas of the cranial nerve VII–XII demonstrate the same rarity, behavior and

imaging findings as the malignant schwannomas of the cranial nerve III–VI (see Sect. 5.5 for details).

5.9 Mimics of Malignant Posterior Skull Base Lesions

Congenital cholesteatoma is a rare disease arising from aberrant ectoderm that is trapped during embryogenesis within the temporal bone (Robert et al. 1995). Histologically, the lesion is lined with stratified squamous epithelium and filled with debris. It typically presents in children and young adults. It can occur anywhere within the temporal bone; when located in the petrous apex it might simulate a malignant lesion of the skull base. Petrous apex congenital cholesteatomas present with facial nerve palsy, sensorineural hearing loss and/or vertigo. On CT, a hypodense, non-enhancing expansile mass is seen with variable degree of bony destruction. Congenital cholesteatoma is usually low to intermediate in signal intensity on T1- and high signal intensity on T2-weighted images (Fig. 26a–c). Presence of restricted diffusion on DWI has also been reported which is not surprising as cholesteatomas histologically resemble epidermoid tumors (Fig. 26d; Aikele et al. 2003). The use of non- echo-planar DWI sequence is recommended in this area as it allows for thinner section thickness and higher imaging matrix with less associated susceptibility artifacts (De Foer et al. 2006). Surgical excision is the treatment of choice and recurrent disease is common with subtotal resection. In such patients, non-echo-planar DWI has shown to be a promising tool for evaluation of residual or recurrent disease as an alternative to exploratory second-look surgery (Dhepnorrarat et al. 2009; De Foer et al. 2010).

Cholesterol granuloma represents an accumulation of granulation tissue intermixed with blood products and cholesterol crystals within the middle ear or petrous apex (Farrior et al. 1981). Patients with cholesterol granuloma classically have a long-standing history of chronic otitis media. Lesions in the petrous apex are often quiet large at the time of diagnosis and may therefore present with hearing loss, tinnitus and/or cranial neuropathies (Goldofsky et al. 1991). On CT, cholesterol granulomas present as expansile, well-defined masses (Fig. 27a; Greenberg et al. 1988). When large, the site of origin might be difficult to determine making distinction to other types of petrous apex lesions, in particular petrous apex aneurysm, difficult. As cholesterol granulomas are often large at the time of initial scanning, CT images often show bony gaps that may be mistaken for bone destruction or erosions suggesting an aggressive or malignant lesion. On MRI, cholesterol granulomas are classically of increased signal intensity on the T1- and T2-weighted images, with no or minimal peripheral enhancement following contrast administration (Fig. 27b). Cholesterol cysts are essentially identical to cholesterol granulomas but occur in the absence of chronic middle ear disease. Mucoceles of the petrous apex share the same imaging characteristics as cholesterol granulomas on CT, but usually demonstrate decreased signal intensity on T1-weighted images. Mucoceles of the petrous apex are very rare and are felt to be related to post-inflammatory obstruction. All of these lesions are usually treated with surgical drainage.

Internal carotid artery aneurysms can occur within the cavernous sinuses, causing remodeling of the adjacent sphenoid bone, or within the petrous bone. The cavernous sinus aneurysms are more common and usually do not demonstrate a diagnostic dilemma. Petrous segment internal carotid aneurysms, in contrast, are rare. They can be congenital, post-traumatic or post-infectious in etiology (Liu et al. 2004). Aneurysms in this location are usually asymptomatic and are incidentally found on CT or MR studies performed for other indications. In symptomatic patients, symptoms are primarily non-specific in nature (headaches) or related to local mass effect (cranial neuropathies, Horner's syndrome or tinnitus). Embolic events have not been associated with petrous segment aneurysm even with larger mural thrombus formation (Liu et al. 2004). On CT, they usually present as an expansile mass with marked enhancement following intravenous contrast administration. The degree and homogeneity of enhancement depends upon the amount of mural thrombus and the size of patent lumen (Fig. 28). If no intravenous contrast is given, they may mimic a cholesterol granuloma, cholesterol cyst or a petrous apex mucocele. Close search for the internal carotid canal within the petrous bone and evaluation of the vector of the associated bone remodeling usually results in correct diagnosis. Contrast-enhanced CT and/or CT angiography might be then performed to confirm the

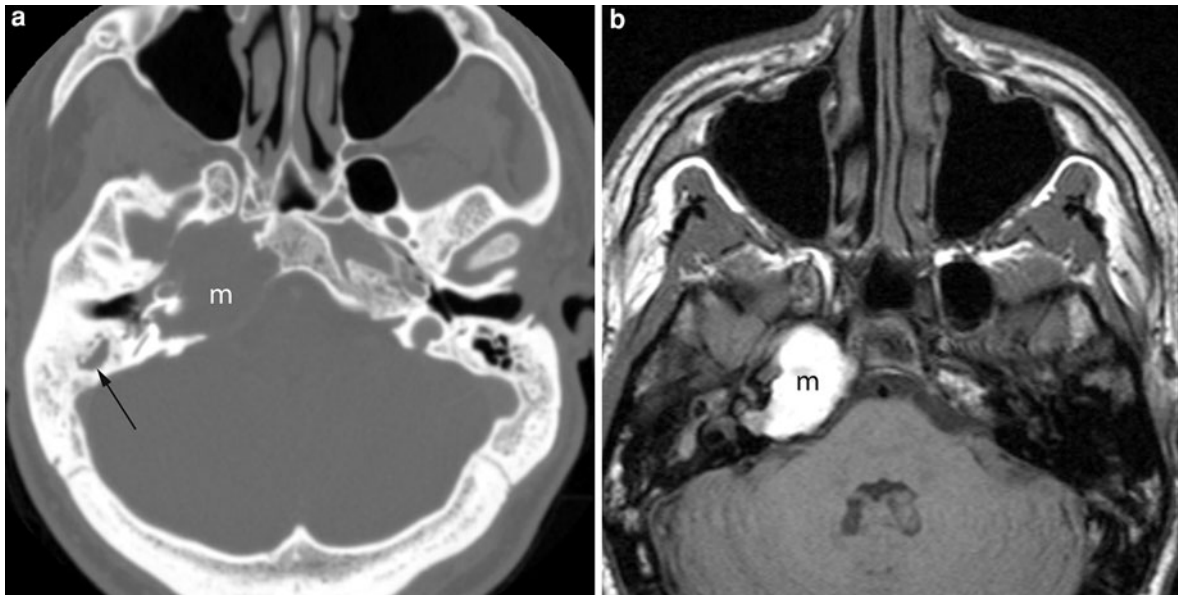

Fig. 27 Axial CT displayed in bone window (**a**) shows a large lytic lesion (*m* in **a**) centered within the petrous apex without signs of cartilageous matrix to suggest a chondrosarcoma. The non-contrast enhanced T1-weighted image in axial plane (**b**) shows spontaneous very high signal intensity of the mass (*m* in **b**) that is characteristic of cholesterol granulomas in contrast to the low to intermediate signal intensity seen in chondrosarcomas that occur in the same location. In addition, there is a small amount of fluid (*arrow* in **a**) present in the mastoid air cells on the right supporting the diagnosis of cholesterol granuloma

diagnosis and to classify the type of the aneurysms (Fig. 28). On MR, petrous apex aneurysms usually present with mixed signal intensity and enhancement pattern, related to the turbulent flow within the aneurysmal segment (Fig. 28). Even MR angiography is usually difficult to interpret as the turbulent flow causes signal drop-out due to reentry phenomenon or thrombus formation that underestimates the size or makes the aneurysm difficult to appreciate at all. This constellation of imaging findings may result in misdiagnosis of the aneurysm as a non-vascular benign and/or malignant skull base lesion. In the instance of present flow voids within the aneurysm, the aneurysm might be completely missed as the difference in signal intensity to adjacent petrous apex, in particular when the petrous apex is aerated, might be very small and therefore not appreciable to the radiologist's eye. The bottom line is that internal carotid artery aneurysms in this location might pose a diagnostic dilemma and the radiologist should consider it every time a petrous apex lesion is observed on CT or MRI to prevent a potential biopsy with usually fatal outcome. The treatment of petrous segment aneurysm remains challenging, in particular when the patient has no or minimal symptoms. Currently, a "wait and see" approach is applied to this latter patient group as these types of aneurysms do not suffer life-threatening bleeding episodes. Endovascular intervention (balloon or coil occlusion of the internal carotid artery and/or stent placement) or surgical trapping with revascularization bypass is currently reserved for symptomatic patients (Liu et al. 2004).

Petrous apicitis is usually caused by otitis media that extended anteromedially into the aerated petrous apex cells without or with progression to osteomyelitis in the early and delayed stages, respectively. Usually, the patients present with fever reflecting the acute nature of the infection in combination with some or all of the symptoms of the Gradenigo's triad (see Sect. 3) (Gradenigo 1904). In the early stages, obliteration of the petrous apex air cells with fluid, in association with otomastoid disease is seen. In the later stages, additional bony destruction with trabecular breakdown and cortical erosions is present, reflecting the degree of underlying osteomyelitis (Fig. 29a). All these changes are readily visible on CT. Petrous apicitis is prone for intracranial complications such as epidural or brain abscess formation,

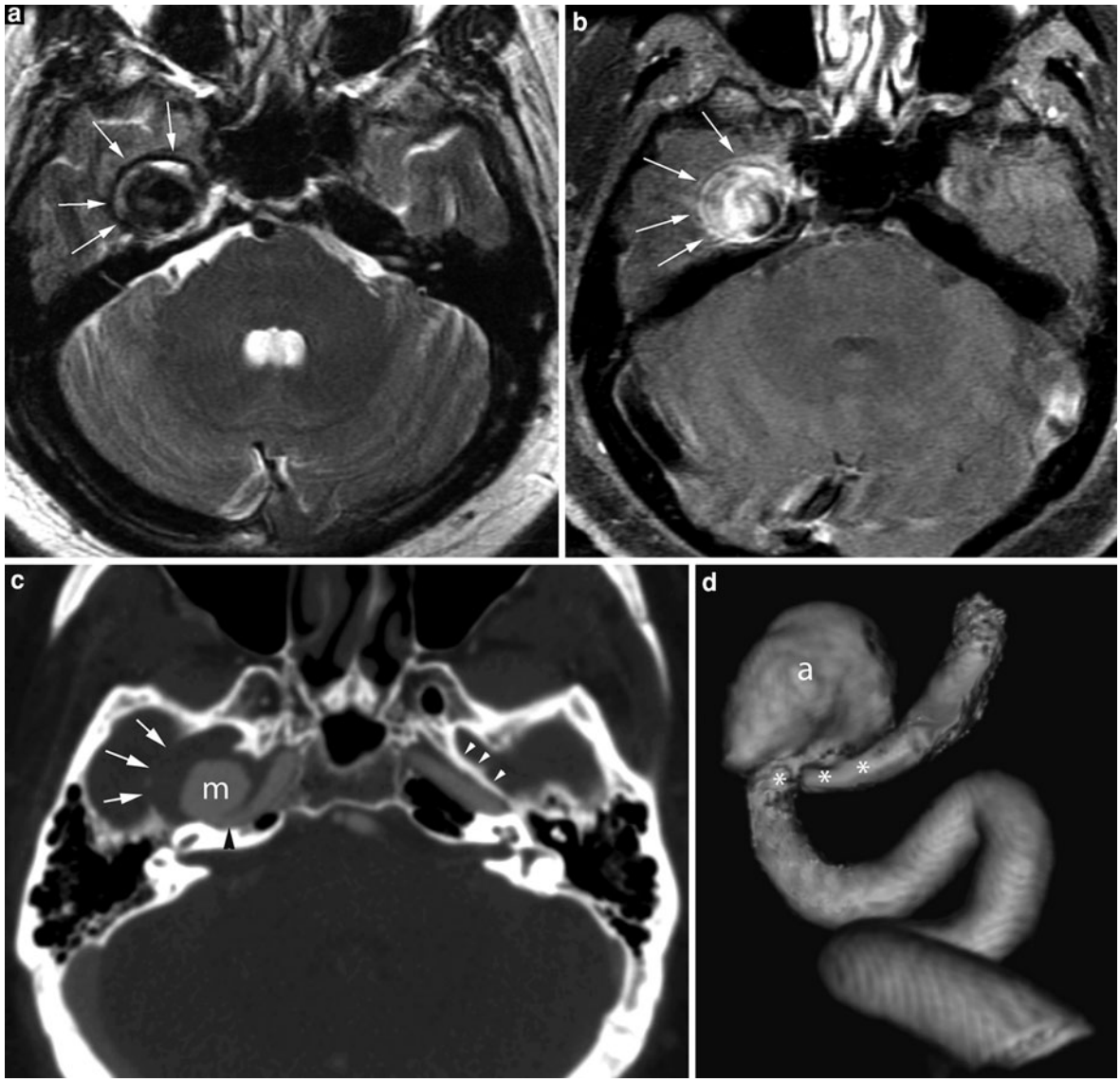

Fig. 28 These images are from a 76-year-old male patients who underwent MR examination for dementia. Axial T2-weighted image (**a**) shows a round and well-defined mass (*arrows* in **a**) of mixed signal intensity centered within the petrous apex. The mass (*arrows* in **b**) shows marked heterogeneous enhancement on the contrast-enhanced fat suppressed T1-weighted image (**b**). The imaging findings were therefore suspicious for an aneurysm of the petrous segment of the internal carotid artery and the patient underwent CT angiography for further evaluation. The contrast-enhanced source image displayed in an intermediate window (**c**) shows extensive lateral bowing of the lateral wall of the internal carotid canal on the right (*white arrows* in **c**) when compared to the left (*white arrowheads* in **c**) caused by a centrally markedly enhancing mass (*m* in **c**) that is contiguous with the internal carotid artery (*black arrowheads* in **c**). The gap between the enhancing central component (*m* in **c**) and the bony bowing (*white arrows* in **c**) reflects the degree of mural thrombus. The maximal intensity projection (MIP) image (**d**) nicely displays the patent portion of the saccular aneurysm (*a* in **d**) arising from the petrous segment of the internal carotid artery (*stars* in **d**)

subdural empyema, meningitis and sinus thrombosis or thromboplebitis (Fig. 29b). These possible complications are usually better delineated with MR imaging. Petrous apicitis, in particular when associated with osteomyelitis or intracranial complications, represents a surgical emergency requiring

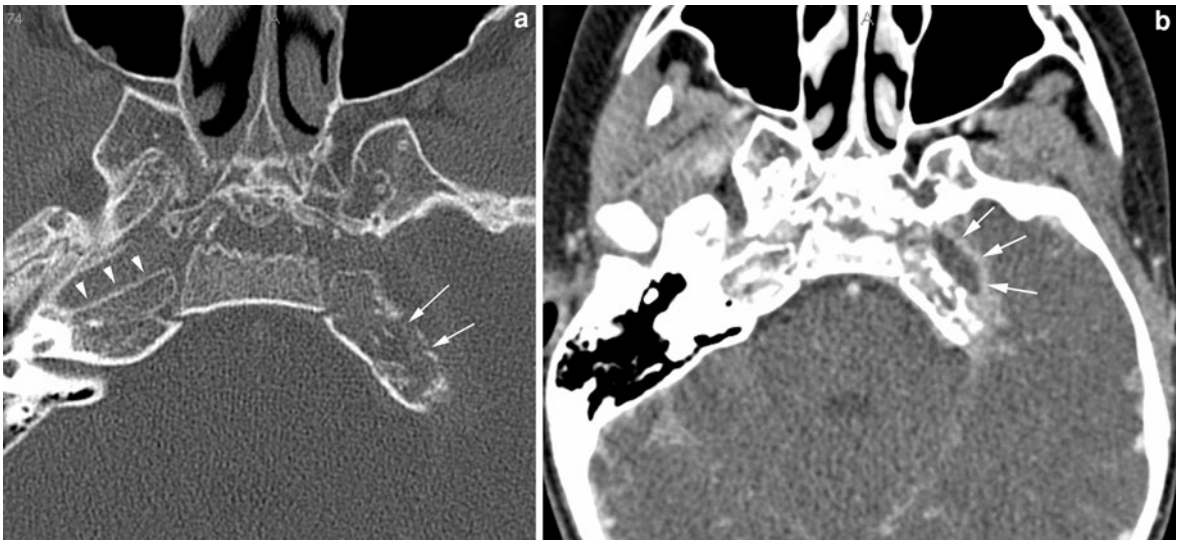

Fig. 29 Axial CT image displayed in bone window (**a**) demonstrates marked dehiscence of the bony cortex (*arrows* in **a**) and fragmented appearance of the petrous apex on the left when compared to the right (*arrowheads* in **a**). The contrast-enhanced axial CT image displayed in soft tissue window shows an extra-dural fluid accumulation with marked ring enhancement (*arrows* in **b**). The constellation of the imaging findings together with fever and signs of otitis media on clinical examination are consistent with petrous apicitis complicated by an epidural abscess that was surgically proven

debridement of the petrous apex and drainage of possible abscesses or empyemas. However, recently, successful conservative treatment of uncomplicated petrous apicitis with new antibiotics has been reported (Burston et al. 2005).

6 Imaging Protocols

In view of the broad variety of lesions that can involve the skull base, it is not surprising that there is no single imaging protocol that fits all these entities. The imaging protocol will primarily depend upon availability, presenting symptoms, patient's history and extent of tumor. Overall, CT is usually the study of first choice as it is widely available and easily accessible. Based on symptoms, MR should be the initial diagnostic study for patients with cranial neuropathies, while CT is primarily reserved as a screening tool for more non-specific symptoms such as headaches and dizziness. Presence of risk factors for a certain disease process (e.g. chronic otomastoiditis or neurofibromatosis), or a history of underlying malignancy in combination with the clinical presentation, might raise the suspicion for a specific entity that it is better evaluated with one or the other imaging tool. The extent of the tumor is usually unpredictable based on clinical examination alone and therefore, review of the images while the patient is still on the scanner with immediate modification of the imaging protocol represents the most optimal work-up of patients with skull base lesions. Despite most optimal image quality a significant number of patients will end up with both—CT and MR—studies for narrowing of the differential diagnostic considerations and better delineation of the tumor margins (Figs. 13, 18, 21, 22).

Although no specific protocol is given here, the following issues need to be considered or followed to facilitate the most optimal quality of a cross-sectional study: CT and MRI should be obtained as a high resolution study with a small field of view (8–14 cm) that is coned down to the area of interest, such as the central skull base or temporal bone. The images should be performed with contiguous slices. It is recommended that CT images are acquired with a slice thickness of 1 mm or less in bone algorithm for optimal display of the bony details of the skull base. In the era of interactive capabilities of the picture archive computer system (PACS) such thin sections are also desirable in soft tissue algorithm to allow high quality multi-planar reformations that facilitate

better delineation of the lesion from adjacent anatomical structures. In contrast, such thin slices are not feasible nor desirable with MR, as the signal to noise would be too low and/or the imaging time too long. Therefore, MR images should be obtained with a slice thickness of 3 mm (Casselman 2005). When a large lesion is present, the slice thickness might need to be increased to 4 mm to be able to cover the entire tumor in a reasonable time frame.

High resolution fast spin-echo T2- and standard T1-weighted images, without and with intravenous contrast administration sequences, should be performed in axial and coronal planes (Casselman 2005). Some tumors also benefit from sagittal imaging, such as chordomas. The standard T1-weighted images without contrast agent are most sensitive for bony invasion, while the T2-weighted images are very helpful in delineation of the outer tumor margins (Figs. 13a, b, 23). Post-contrast agent T1-weighted images are most useful for evaluation of involvement of adjacent soft tissues (Fig. 23). Utilization of fat suppression techniques in the skull base is controversial as it is hampered by loss of most of the anatomical landmarks, and is predisposed for susceptibility artifacts. In addition, the suppression of fat makes the typically high signal difference between tumor and adjacent fatty bone marrow disappear on the plain images, and the detectibility of a lesion on the contrast-enhanced images will depend upon the degree of intra-lesional contrast accumulation. Therefore, it is advisable to obtain standard plain T1-weighted images without fat suppression in at least one imaging plane (preferentially the axial plane) that would supplement the fat suppressed images. Additional imaging sequences such as heavily T2-weighted high resolution volumetric acquisitions or MR angiography/venography might also be considered for further evaluation of the cisternal portions of the cranial nerves or of the intracranial vasculature, respectively. It is also recommended to perform larger field of view images (20–22 cm) through the entire head in non-enhanced T1 and fluid attenuation inversion recovery (FLAIR) weighing that could serve as an overview for optimal positioning of the subsequently acquired high resolution images; these would allow detectibility of additional lesions as well as possible complications related to the skull base mass such as infarction at the same time. Additional DWI through the entire head might not only further characterize the age of potential infarction, but also narrow the differential diagnosis in some instances.

7 Radiologist's Role

The radiologist's main role pretreatment is the delineation of the extent of the suspected malignant skull base lesion, including delineation of possible involvement of the neurovascular structures. Narrowing of the differential diagnostic considerations is certainly desirable but not as critical as the tumor extent. The radiologist might offer biopsy of a lesion when a soft tissue component is present below the skull base that is accessible for biopsy with CT guidance. Central skull base lesions can be often reached by placement of a guiding needle through the mandibular notch or through the buccal space along the anterior margin of the mandibular ramus. However, CT guided biopsy of the bony skull base itself is difficult due to the high frequency of traversing nerves and vessels.

During the treatment phase, the interventional radiologist might perform intra-arterial embolization of a vascular tumor prior to surgical resection or treat a petrous segment internal carotid aneurysm with balloon/coil occlusion.

Posttreatment imaging is critical as surgical resections are often subtotal in extent and radiation therapy may leave residual masses of unknown activity. To facilitate the radiologist's ability to detect recurrent tumor as soon as possible, it is advisable to obtain a baseline CT and/or MR study approximately 6 weeks following treatment, and to perform the subsequent follow-up examinations with the same imaging protocol and technique.

References

Aikele P, Kittner T, Offergeld C, Kaftan H, Huttenbrink KB, Laniado M (2003) Diffusion-weighted MR imaging of cholesteatoma in pediatric and adult patients who have undergone middle ear surgery. Am J Roentgenol 181: 261–265

Azar-Kian B, Sarwar M, Marc JA, Schlechter MM (1974) Intraosseous meningioma. Neuroradiology 6:246–253

Barber B, Ingram M, Khan S, Bano G, Hodson S, Vlahos I (2011) Clinicoradiological manifestations of paraganglioma syndromes associated with succinyl dehydrogenase enzyme mutation. Insights Imaging 2(4):431–438

Bolger WE, Reger C (2003) Temporal lobe encephalocele appearing as a lytic lesion of the skull base and pterygoid process. Ear Nose Throat J 82:268–272

Bomanji JB, Hyder SW, Gaze MN, Gacinovic S, Costa DC, Coulter C, Ell PJ (2001) Functional imaging as an aid to decision-making in metastatic paraganglioma. Br J Radiol 74:266–269

Bourgouin PM, Tampieri D, Robitaille Y, Robert F, Bergeron D, del Carpio R, Melancon D, Ethier R (1992) Low-grade myxoid chondrosarcoma of the base of the skull: CT, MRI, and histopathology. J Comput Assist Tomogr 16:268–273

Brewis C, Bottrill ID, Wharton SB, Moffat DA (2000) Metastases from glomus jugulare tumours. J Laryngol Otol 114:17–23

Brodeur GM, Castleberry RP (2001) Neuroblastoma. In: Pizzo PA, Poplack DG (eds) Principles and practice of pediatric oncology. Lippincott Williams & Wilkins, Philadelphia, p 796

Burston BJ, Pretorius PM, Ramsden JD (2005) Gradenigo's syndrome: successful conservative treatment in adult and paediatric patients. J Laryngol Otol 119:325–329

Carlotti CG Jr, Drake JM, Hladky JP, Teshima I, Becker LE, Ruthka JT (1999) Primary Ewing's sarcoma of the skull in children utility of molecular diagnostics, surgery and adjuvant therapies. Pediatr Neurosurg 31:307–315

Casselman JW (2005) The skull base: tumoral lesions. Eur Radiol 15:534–542

Chong VFH, Fan YF (1998) Radiology of the sphenoid bone. Clin Radiol 53:882–893

Choyke PL, Glenn GM, Walther MM, Patronas NJ, Linehan WM, Zbar B (1995) Von Hippel Lindau disease: genetic, clinical and imaging features. Radiology 146:629–642

Crawford TS, Kleinschmidt-DeMasters BK, Lillehei KO (1995) Primary intraosseous meningioma (Case report). J Neurosurg 83:912–915

Cummings TJ, George TM, Fuchs HE, McLendon RE (2004) The pathology of extracranial scalp and skull masses in young children. Clin Neuropathol 23:34–43

De Foer B, Vercruysse JP, Pilet B, Michiels J, Vertiest R, Pouillon M, Somers T, Casselman JW, Offeciers E (2006) Single-shot, turbo spin-echo, diffusion-weighted imaging versus spin-echo-planar, diffusion-weighted imaging in the detection of acquired middle ear cholestatoma. Am J Neuroradiol 27:480–482

De Foer B, Vercruysse JP, Bernaerts A et al (2010) Middle ear cholesteatoma: non-echo-planar diffusion-weighted MR imaging versus delayed gadolinium-enhanced T1-weighted MR imaging—value in detection. Radiology 255:866–872

Dhepnorrarat RC, Wood B, Rajan GP (2009) Postoperative non-echo-planar diffusion-weighted magnetic resonance imaging changes after cholesteatoma surgery: implications for cholesteatoma screening. Otol Neurotol 30:54–58

DiNardo LJ, Wetmore RF (1989) Head and neck manifestations of histocytosis-X in children. Laryngoscope 99:721–724

Erdem E, Angtuaco EC, Van Hemert R, Park JS, Al-Mefty O (2003) Comprehensive review of intracranial chordomas. Radiographics 23:995–1009

Evans HL, Ayala AG, Romsdahl MM (1977) Prognostic factors in chondrosarcoma of bone: a clinicopatholgogic analysis with emphasis on histologic grading. Cancer 40:818–831

Farrior B, Kampsen E, Farrior JB (1981) The positive pressure of cholesterol granuloma idiopathic blue eardrum: differential diagnosis. Laryngoscope 91:1286–1296

Filippi CG, Edgar MA, Ulug AM, Prowda JC, Heier LA, Zimmerman RD (2001) Appearance of meningiomas on diffusion-weighted images: correlating diffusion constants with histopathologic findings. Am J Neuroradiol 22:65–72

Forsyth PA, Cascino TL, Shaw EG, Scheithauer BW, O'Fallon JR, Dozier JC, Piepgras DG (1993) Intracranial chordomas: a clinocopathological and prognostic study of 51 cases. J Neurosurg 78:741–747

Gandour-Edwards R, Kapadia SB, Janecka IP, Martinez AJ, Barnes L (1995) Biologic markers of invasive pituitary adenomas involving the sphenoid sinus. Mod Pathol 8:160–164

Garg V, Temin N, Hildenbrand P, Silverman M, Catalano PJ (2010) Inflammatory pseudotumor of the skull base. Otolarngol Head Neck Surg 142:129–131

Garland LH (1945) Osteogenic sarcoma of the skull. Radiology 45:45–48

Goldofsky E, Hoffman RA, Holliday RA, Cohen NL (1991) Cholestrol cyst of the temoporal bone: diagnosis and treatment. Ann Otol Rinol Laryngol 100:181–186

Gorham LW, Wrighte AW, Schulz HH, Maxon FC (1954) Disappearing bones: a rare form of massive osteolysis, report of two cases, one with autopsy findings. Am J Medicine 17:674–681

Gormley WB, Tomecek FJ, Qureshi N, Malic GM (1994) Craniocerebral epidermoid and dermoid tumours: a review of 32 cases. Acta Neurochir (Wien) 128:115–121

Gradenigo G (1904) Sulla leptomeningite circonscritta e sulla paralisi dell' abducenta di origine otitica. Giornale dell'Accademia di medicina di Torino 10:59–84

Greenberg JJ, Oot RF, Wismer GL, Davis KR, Goodman ML, Weber AE, Montgomery WW (1988) Cholesterol granuloma of the petrous apex: MR and CT evaluation. Am J Neuroradiol 6:1205–1214

Guo AC, Cummings TJ, Dash RC, Provenzale JM (2002) Lyphomas and high-grade astrocytomas: comparison of water diffusibility and histological characteristics. Radiology 224:177–183

Hassounah M, Al-Mefty O, Akhtar M, Jenkins JR, Fox JL (1985) Primary cranial and intracranial chordosarcoma: a survey. Acta Neurosurgica 78:123–132

Howarth DM, Gilchrist GS, Mullan BP, Wiseman GA, Edmonson JH, Schomber PJ (1999) Langerhans cell histocytosis: diagnosis, natural history, management, and outcome. Cancer 85:2278–2290

Inserra MM, Pfeister M, Jackler RK (2004) Anatomy involved in the jugular foramen approach for jugulotympanic paragrangioma resection. Neurosurg Focus 17:41–44

Jabre A, Tabaddor R, Samaraweera R (2000) Transphenoidal meningoencephalocele in adults. Surg Neurol 54:183–187

Joseph M, Rajshekhar V, Chandy MJ (2004) Haematopoietic tissue presenting as a sphenoid sinus mass: case report. Neuroradiology 42:153–154

Kaufman B, Bellon EM (1973) The trigeminal nerve cistern. Radiology 108:597–602

Kozlowski K, Cambell J, Mc Alister W, Babyn P, Cama A, Masel J, Pelizza A, Taccone A (1991) Rare primary cranial

vault and base of skull tumours in children: report of 30 cases and short literature review. Radiol Med 81:213–224
Laigle-Donadey F, Taillibert S, Martin-Duverneuil N, Hildebrand J, Delattre JY (2005) Skull-base metastases. J Neurooncol 75:63–69
Lang FF, Macdonald OK, Fuller GN, DeMonte F (2000) Primary extradural meningiomas: a report of nice cases and review of literature from the era of computerized tomography scanning. J Neurosurg 93:940–950
Layer G, Steudal A, Schuller H, van Kaick G, Grunwald F, Riser M, Schild HH (1999) Magnetic resonance imaging to detect bone marrow metastases in the initial staging of small cell lung carcinoma and breast carcinoma. Cancer 85:1004–1009
Liu JK, Gottfried ON, Amini A, Couldwell WT (2004) Aneurysms of the petrous internal carotid artery: anatomy, origins, and treatment. Neursurg Focus 17:1–9
Loevner LA, Tobey JD, Yousem DM, Sonners AI, Hsu WC (2002) MR imaging characteristic of cranial bone marrow in adult patients with underlying systemic disorder compared with healthy control subjects. Am J Neuroradiol 23:248–254
Luff DA, Simmons M, Malik T, Ramsden RT, Reid H (2002) Endolymphatic sac tumours. J Laryngol Otol 116:398–401
Mascalchi M, Filippi M, Floris R, Fonda C, Gasparotti R, Villari N (2005) Diffusion-weighted MR of the brain: methodology and clinical application. Radiol Med (Torino) 109:155–197
Miller C, Lloyd TV, Johnson JC, Hunt WE (1978) Eosinophilic granuloma of the base of the skull: case report. J Neurosurg 49:464–466
Moore KL, Dalley AF (1999) Head and neck. In: Moore KL, Dalley AF (eds) Clinically oriented anatomy, 4th edn. Lippincott Williams & Wilkins, Philadelphia, pp 1093–1096
Mukherji SK, Castillo M (1996) Adenocarcinoma of the endolymphatic sac: imaging features and preoperative embolization. Neurordaiology 38:179–180
Mukherji SK, Baggett HC, Alley J, Carrasco VH (1998) Enlarged cochlear aqueduct. Am J Neuroradiol 19:330–332
Price T, Fayad G (2002) Abducens nerve palsy as the sole presenting symptom of petrous apicitis. J Laryngol Otol 116:726–729
Ragel BT, Couldwell WT (2004) Pituitary carcinoma: review of the literature. Neurosurg Focus 16:1–9
Rao AB, Koeller KK, Adair CF (1999) From the archives of the AFIP: Paragangliomas of the head and neck: radiologic–pathologic correlation. Radiographics 19:1605–1632
Robert Y, Carcasset S, Rocourt N, Hennequin C, Dubrulle F, Lamaitre L (1995) Congenital cholesteatoma of the temporal bone: MR findings and comparison with CT. Am J Neuroradiol 16:755–761
Rueda-Franco F, Lopez-Correla E (1995) Sarcomas in the central nervous system of children. Pediatric Neurosurg 22:49–56
Salvati M, Ciappetta P, Capone R, Santoro R, Raguso M, Raco A (1993) Osteosarcoma of the skull in a child: a case report and review of the literature. Childs Nerv Syst 9:437–439
Satter EK, High WA (2008) Langerhans cell histiocytosis: a review of the current recommendations of the Histiocyte Society. Pediatr Dermatol 25:291–295
Schmalfuss IM (2009) Petrous Apex. Neuroimaging Clin N Am 19:367–391
Schmalfuss IM, Camp M (2008) Skull Base: normal variants and Pseudolesions. Eur Radiol 18:1232–1243
Sen C, Hague K, Kacchara R, Jenkins A, Das S, Catalano P (2001) Jugular foramen: microscopic anatomic features and implications for neural preservation with reference to glomus tumors involving the temporal bone. Neurosurgery 48:838–847
Shinoda J, Kimura T, Funakoshi T, Iwata H, Tange K, Kasai C, Miyata Y (1993) Primary osteosarcoma of the skull. J Neurooncol 17:81–88
Smirniotopoulos JG, Chiechi MV (1995) Teratomas, dermoid, and epidermoids of the head and neck. Radiographics 15:1437–1455
Stone JA, Cooper H, Castillo M, Mukherji SK (2001) Malignant schwannoma of the trigeminal nerve. Am J Neuroradiol 22:505–507
Tauber M, van Loveren HR, Jallo G, Romano A, Keller JT (1999) The enigmatic foramen lacerum. Neurosurgery 44:386–391
Tokgoz N, Oner YA, Kaymaz M, Ucar M, Yilmaz G, Tali TE (2005) Primary intraosseous meningioma: CT and MRI appearance. Am J Neuroradiol 26:2053–2056
Tunaci M, Tunaci A, Engin G, Ozkorkmaz B, Dincol G, Acunas G, Acunas B (1999) Imaging features of thalassemia. Eur Radiol 9:1804–1809
Turner OA, Laird AT (1966) Meningioma with traumatic etiology. J Neurosurg 24:96–98
Utz JA, Krandorf MJ, Jelinek JS, Moser RP Jr, Berrey BH (1989) MR appearance of fibrous dysplasia. J Comput Assist Tomogr 13:845–851
Van Tassel P, Lee YY, Ayala A, Carrasco CH, Klima T (1991) Case report 680: intraosseous meningioma of the sphenoid bone. Skeletal Radiol 20:383–386
Whitehead RE, Melhem ER, Kasznica J, Eustace S (1998) Telangiectatic osteosarcoma of the skull base. Am J Neuroradiol 19:754–757
Williams LS, Schmalfuss IM, Sistrom CL, Inoue T, Tanaka R, Seoane ER, Mancuso AA (2003) MR imaging of the trigeminal ganglion, nerve and the perineural vascular plexus: normal appearance and variants with correlation to cadaver specimens. Am J Neuroradiol 24:1317–1323
Williamson RA, Paueksakon P, Coker NJ (2003) Inflammatory pseudotumor of the temporal bone. Otol Neurotol 24:818–822
Yildirim T, Agildere AM, Oguzkurt L, Barutcu O, Kizilkilic O, Kocak R, Alp Niron E (2005) MRI evaluation of cranial bone marrow signal intensity and thickness in chronic anemia. Eur J Radiol 53:125–130